

Chapter 23

Linear elasticity with *microstructure and size effects*

G. Exadaktylos

School of Mineral Resources Engineering, Technical University of Crete, Chania, Greece

Abstract: The revisiting of some fundamental problems of rock mechanics, such as cracks in stressed rocks, propagation of surface waves, beam bending and axial splitting among others, viewed in the light of a strain gradient elasticity theory, reveals the necessity of enriching elasticity of rocks with length parameters to model surface energy of free surfaces and predict non-classical dispersion phenomena and size effects. After a brief review of the formalism and applications of a linear elasticity theory with microstructure for the study of static and dynamic problems, two problems are further presented here, namely the bending of beams and the axial splitting of deep geological layers. It is demonstrated in both studied problems, that the consideration of internal length scales are responsible for the manifestation of size effects.

I INTRODUCTION

I.1 Brief notes on the size effects of strength of materials

The size effect exhibited by the strength of solids for otherwise geometrically similar specimens, is not new in the context of the strength of brittle materials. Long before Griffith (1921) presented his theory, Karmarsch¹ in 1858 has proposed an empirical size effect law based on a best-fitting procedure of experimental data of tension tests on cylindrical metal wires with different diameters. This size effect is mentioned in the celebrated Griffith's paper and was applied successfully by him to fit experimental data referring to tension tests of glass fibers presented in Table V of his paper, namely

$$\sigma_t = 154.44 + \frac{17.27}{d} \quad (1)$$

in which the diameter of the rods d is expressed in 0.001 mm and the tensile strength σ_t in MPa. The best-fitted size-effect law given by Equation 1 on the experimental data is shown in Figure 1.

In most technical brittle materials, such as rocks, concretes and ceramics, the domains in the vicinity of the highly stress point participate in the force transmission more intensively than according to the local linear theory of elasticity (the term 'local' is explained below); during the endangered point itself is somewhat relieved; this self-

1 "Mittheilungen des gew. Ver. Für Hannover", 1858, pp. 138–155.

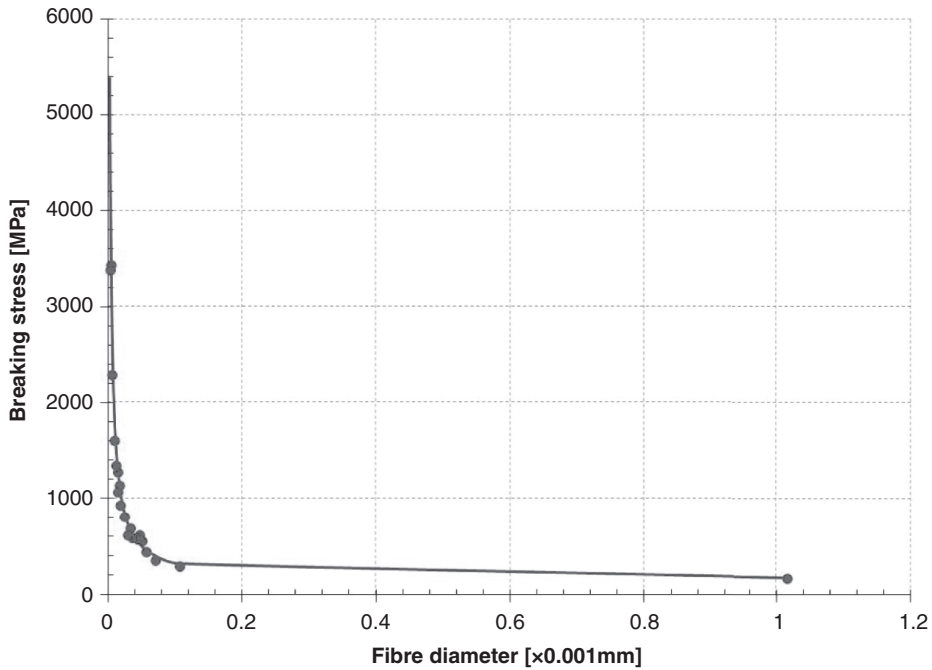


Figure 1 Size effect exhibited by the tensile strength of glass fibers (circles) tested by Griffith (1921) and best-fitted inverse diameter relationship (continuous line).

support-effect of a stress raiser is taken into account by the stress-mean-value theory and the more elegant gradient elasticity theory with surface energy that is presented later.

First, let us make a remark on the averaging procedure that is inherent in all local continuum mechanics theories. A simple example is to consider an one-dimensional case of a field, $y=f(x)$, whose mean value is computed over a small but finite averaging length L – corresponding to the representative elementary volume – around a point x , that is

$$\langle y \rangle = \frac{1}{L} \int_{-L/2}^{L/2} f(x + \xi) d\xi \tag{2}$$

If the field $f(x)$ varies linearly in the considered region around x , then it is approximated locally by a linear function, using an 1-term Taylor series expansion of the function f around point x , *i.e.*

$$f(x + \xi) \approx f(x) + \xi f'(x) \tag{3}$$

In the trivial case of a constant field, then the first and all higher derivatives vanish and indeed the local value coincides with the average value. Also it is true in case when the field varies locally linearly. Indeed we may then identify the field with its mean value over the considered averaging length, because by following the ‘trapezoidal’ integration rule, the value of a linearly varying field in the midpoint of the sampling interval is equal to its mean value in that interval

$$y = \langle y \rangle \tag{4}$$

that is to say, in this case the ‘local’ value y and the ‘non-local’ value $\langle y \rangle$ coincide. In the classical theories of elasticity, plasticity and damage mechanics, the failure criterion is expressed in terms of stresses and strains, and no characteristic length scale L is present. Hence, they are all “local theories”. However, for quadratically varying fields, we have to approximate the stress function at least by a two-term Taylor series expansion around point x , *i.e.*

$$f(x + \xi) \approx f(x) + f'(x)\xi + \frac{1}{2}f''(x)\xi^2 + \frac{1}{6}f'''(x)\xi^3 + o(\xi^4) \tag{5}$$

We notice that in the midpoint integration rule the effect of the first derivative is null. Thus for ‘quadratically’ varying fields, computational rule described by Equation 4 must be enhanced, so as to incorporate the effect of the curvature

$$y = \langle y \rangle - \left. \frac{L^2}{24} \frac{d^2y}{dx^2} \right|_x + O(L^4) \tag{6}$$

Field theories which are based on averaging rules that include the effect of higher gradients are called higher gradient or ‘nonlocal’ theories. In particular, the above rule of Equation 6 represents a 2nd gradient or grade-2 rule, and can be readily generalized in two and three dimensions. One of the first researchers who proposed a gradient theory based on the mean value of the nominal stress along the potential fracture path was Neuber (1936). More specifically Neuber proposed a stress-mean-value taken over a finite length L normal to the surface within the range of high stress concentration. This so-called ‘fictive’ length of the elastic material represents an additional material constant apart say, from the two elasticity constants for a linear elastic and isotropic material. According to this argument the nominal stress σ_n can be found from the formula

$$\sigma_n = \frac{1}{L} \int_{r=R}^{R+L} \sigma dr \tag{7}$$

in which r denotes the radial distance from the notch tip, $r=R$ is the notch boundary, and σ is the so-called ‘comparison’ stress that enters a suitable strength hypothesis.

In the case of mode-III (anti-plane shear) crack the nominal stress is derived by the following formulae according to definition of Equation 7 and the valid asymptotic expression for the comparison stress σ_{yz}

$$\sigma_n = \frac{1}{L} \int_{r=0}^L \sigma_{yz}(r, 0) dr; \quad \sigma_{yz} = \frac{K_{III}}{(2\pi r)^{1/2}} \cos \frac{\theta}{2} \tag{8}$$

where K_{III} denotes the mode-III Stress Intensity Factor (SIF) and $Or\theta$ the polar coordinate system with origin at the crack tip. The direct evaluation of the above integral for $\theta = 0^\circ$ gives the result

$$\sigma = \sqrt{\frac{2}{\pi}} \frac{K_{III}}{\sqrt{L}} + o(\sqrt{L}) \tag{9}$$

On the other hand, the exact expression for the comparison stress by employing the Westergaard stress function reads as follows

$$\sigma_{yz} = \text{Re}(Z_{III}), \quad Z_{III} = \frac{\tau_{\infty}(z + \alpha)}{[(\alpha + z)^2 - \alpha^2]^{1/2}}; \quad z = re^{i\theta} \tag{10}$$

and consequently the exact stress along the Ox-axis is given by the expression

$$\sigma_{yz} \Big|_{\theta=0} = \frac{\tau_{\infty}(r + \alpha)}{(r^2 + 2\alpha r)^{1/2}} \tag{11}$$

where τ_{∞} represents the far-field shear stress. In turn, the nominal stress in this case may be found to be

$$\sigma_n = \frac{1}{L} \int_{r=0}^L \sigma_{yz} \Big|_{\theta=0} dr = \tau_{\infty} \sqrt{1 + 2\frac{\alpha}{L}} \tag{12}$$

By requiring that both approaches should lead to the same result, *i.e.*

$$\lim_{r \rightarrow 0} \left[\sqrt{\frac{2}{\pi}} \frac{K_{III}}{\sqrt{L}} = \tau_{\infty} \sqrt{1 + 2\frac{\alpha}{L}} \right] \tag{13}$$

there results

$$\hat{K}_{III} = \sqrt{1 + \frac{1}{2(\alpha/L)}}; \quad K_{III} = \tau_{\infty} \sqrt{\pi \alpha} \tag{14}$$

where \hat{K}_{III} represents the normalized fracture toughness that is derived by dividing the expression for the critical stress intensity factor with the fracture toughness K_{III} predicted by the classical theory. The variation of the normalized fracture toughness \hat{K}_{III} with the ratio α/L - *i.e.* the size effect exhibited by fracture toughness - is illustrated in Figure 2. This means that for long cracks relative to the scale length L one gets the result of Linear Elastic Fracture Mechanics (LEFM); on the other hand, for relatively short cracks the fracture toughness is larger than that predicted by classical LEFM.

1.2 Brief historical remarks on non-local elasticity theories

The classical theory of elasticity requires that the forces between the atoms to fulfill a very strong condition, namely that the range of these forces must be small enough so that the stress (strain) measured at a point depends in the desired approximation only on the stress (strain) in the volume element around this point; hence the term ‘local’ theory. Obviously, if interatomic forces did not reach farther than one atomic distance, a reaction against micro-deformation gradient would not exist and the theory does not

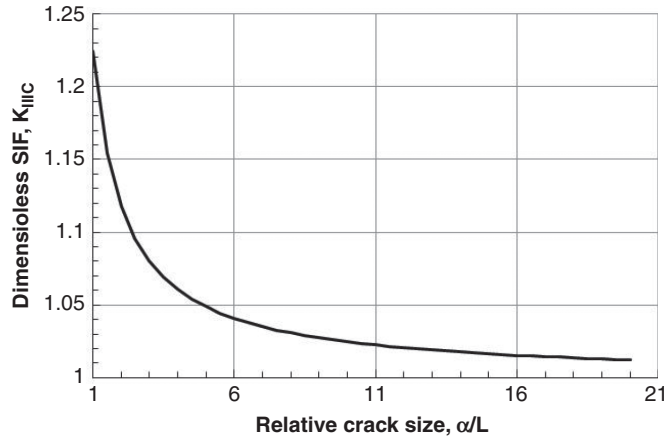


Figure 2 Size effect of the normalized fracture toughness \hat{K}_{IIC} predicted by the stress-mean-value theory.

have an intrinsic length scale; this in turn leads to the undesirable result that a 10 cm slab behaves the same as a 10 m geological bed, and there is no difference between a microcrack and a geological fault. However, since interatomic forces do, in principle, reach farther than one atomic distance, a resistance against micro-deformation gradient will be present, and therefore it is of no question whether gradient-dependent elasticity exists or not. The question is rather *how large* this effect might be.

The fundamental idea of considering not only the first, but also the higher gradients of the displacement field in the expression for the strain energy function of an elastic solid, can be traced back to J. Bernoulli (1654–1705) and L. Euler (1707–1783) in connection with their work on beam theory. In elementary beam theory there are associated two sets of kinematical quantities (a deformation vector and a rotation vector) and two sets of surface loads (tractions and bending couples) with a section of the bar. In plate theory the situation is similar. With the noticeable monograph of Cosserat brothers, Eugène and François (1909), this concept was extended to a 3D continuum, where each point of the continuum is supplied with a set of mutually perpendicular rigid vectors (triad). Generalization of elasticity theory by incorporating the effect of higher gradients of the displacement field into the strain energy density function was systematically studied by them. The novel feature of their theory was the appearance of couple stresses in the equations of motion. An oriented continuum of this type was noted earlier by Voigt (1887) in connection with polar molecules in crystallography. Higher-order gradient and oriented media theories were rediscovered fifty years later in various special forms and degree of complexity. Fifty years after the first publication of the original work of the Cosserat brothers, the basic kinematic and static concepts of the ‘Cosserat’ continuum were reworked in a milestone paper by Guenther (1958). Guenther’s paper marks the rebirth of continuum micro-mechanics in the late 50’s and early 60’s. Following this publication, several hundred papers were published all over the world on that subject. A variety of names have been invented and given to theories of various degrees of rigor and complexity: Cosserat continua or micro-polar

media, oriented media, continuum theories with directors, multi-polar continua, micro-structured or micro-morphic or non-local continua and others. A systematic treatment of elasticity with gradients was given in milestone papers by Mindlin & Tiersten (1962), Mindlin (1964) and Mindlin & Eshel (1968). The common feature of all these studies is that they relate the higher gradients of the displacement field to higher order stresses. Mindlin's work is noteworthy in that his aim was specifically targeted at understanding phenomenologically the effect of microstructure on the deformation of solids. Mindlin's cohesive elasticity theory accounts in a phenomenological manner for molecular forces of cohesion acting upon a body - which are not considered by the classical linear elasticity theory - by including in the potential energy density of an elastic solid the 'modulus of cohesion', which is essentially an initial, homogeneous, self-equilibrating triple stress. However, Mindlin's isotropic grade-3, linear elasticity theory with surface energy, which was further explored, as far as its mathematical potential is concerned, in a comprehensive paper by Wu (1992), includes sixteen material constants plus the classical Lamè's constants. The state-of-the-art at this time was reflected in the collection of papers presented at the historical IUTAM Symposium on the "*Mechanics of Generalized Continua*", in Freudenstadt and Stuttgart in 1967. At the same time practically of publication of the pioneering papers by Mindlin, Professor Germain has encouraged the communication to the French Academy of Sciences of the ideas of Casal (1961) which in turn seem to have inspired Germain's (1973a,b) fundamental papers on the continuum mechanics structure of the grade-2 or higher grade theories. In our paper we want to give full credit to Casal's original idea, who was first to see the connection between surface tension effects and the anisotropic gradient elasticity theory. For this reason we provide here the simplest possible generalization of Casal's constitutive theory that accounts for only two additional material constants having the dimension of length: One, say ℓ , responsible for volumetric energy strain-gradient terms, and another, ℓ' , responsible for surface energy strain-gradient terms. Casal considered the effect of the granular, polycrystalline and atomic nature of materials on their macroscopic response through the concept of internal and superficial capillarity expressed by the material lengths ℓ , ℓ' , respectively, rather than through intractable statistical mechanics concepts. The concept that the surfaces of liquids are in a state of tension is a familiar one, and it is widely utilized. Actually it is known that no skin or thin foreign surface really is in existence at the surface, and that the interaction of surface molecules causes a condition analogous to a surface subjected to tension. The surface tension concept is therefore an analogy, but it explains the surface behavior in such satisfactory manner that the actual molecular phenomena need not be invoked. Of course such ideas are amenable to generalizations of various degrees of complexity. However, one should keep in mind that already the determination of the two material lengths ℓ and ℓ' constitutes a formidable experimental challenge.

The Casal-Mindlin grade-2 theory has been applied for the revisit of several static and dynamic boundary-value problems in Rock Mechanics (Vardoulakis & Sulem, 1995; Vardoulakis *et al.*, 1996; Exadaktylos *et al.*, 1996; Exadaktylos & Vardoulakis, 1998; Exadaktylos, 1998; Exadaktylos & Vardoulakis, 2001a; Aravas, 2011 among others). The consideration of the surface energy in this theory, leads to a constitutive character of the boundary conditions. This strengthens Aifantis' (1992) conjecture of the constitutive character of boundary constraints in materials with microstructure. Hence, the problem of constitutive boundary conditions deserves further attention

from the theoretical, as well as the experimental point of view. Exadaktylos & Vardoulakis (2001a) have shown that the proposed theory is capable: (a) to capture scale effects in indentation and uniaxial tension testing of rocks, and (b) to predict cusping of cracks without recourse to extra assumptions. The present anisotropic gradient elasticity theory although it is basically a grade-2 theory gives rise to surface tension phenomena similar to those captured by Mindlin's (1964; 1965) grade-3 theory. This is demonstrated in Paragraph 1.5.

1.3 Formalism of the Casal-Mindlin microelasticity theory

In this sequel the basic formalism of the grade-2 theory of elasticity are outlined. With respect to a fixed Cartesian coordinate system $Ox_1x_2x_3$, the following *ansatz* for the elastic strain energy density with respect to three kinematic quantities is assumed in an ad hoc manner

$$v = v(\varepsilon_{qr}, \gamma_{qr}, \kappa_{qrs}) \tag{15}$$

where $\varepsilon_{qr} \equiv (1/2)(\partial_r u_q + \partial_q u_r)$ is the usual symmetric infinitesimal macro-strain tensor defined in terms of the displacement vector u_q , $\partial_s \equiv \partial/\partial x_s$, the indices (q,r,s) span the range (1,2,3), $\gamma_{qr} \equiv \partial_q u_r - \psi_{qr}$ is the relative deformation with ψ_{qr} denoting the micro-deformation of a particle in the form of a grain or crystal for a granular or crystalline rock, respectively, (Figures 3a, b), and $\kappa_{qrs} \equiv \partial_q \psi_{rs}$ is the micro-deformation gradient. Then, appropriate definitions for the stresses follow from the variation of v , *i.e.*

$$\tau_{qr} \equiv \frac{\partial v}{\partial \varepsilon_{qr}}, \quad \alpha_{qr} \equiv \frac{\partial v}{\partial \gamma_{qr}}, \quad \mu_{qrs} \equiv \frac{\partial v}{\partial \kappa_{qrs}}, \tag{16}$$

in which τ_{qr} , α_{qr} , μ_{qrs} denote the Cauchy stress (symmetric), relative stress (asymmetric), and double stress tensors, respectively. The twenty-seven components μ_{kij} have the character of double forces per unit area. The first subscript of a double stress μ_{kij} designates the normal to the surface across which the component acts; the second and third subscripts have the same significance as the two subscripts of σ_{ij} . The eight components of the deviator of the couple-stress or couples per unit area formed by the combinations $(1/2)(\mu_{pqr} - \mu_{prq})$ are all equal to zero in the present gradient dependent elasticity theory, whereas all the remaining ten independent combinations $(1/2)(\mu_{pqr} + \mu_{prq})$ are self-equilibrating (Mindlin, 1964). Double force systems without moments are stress systems equivalent to two oppositely directed forces at the same point; such systems have direction but not net force and no resulting moment.

In particular, the theory utilized here can be considered as one of the simplest versions of Casal-Mindlin theory corresponding to the following elastic strain energy density function (Exadaktylos & Vardoulakis, 1998)

$$v = \frac{1}{2} \lambda \varepsilon_{ii} \varepsilon_{jj} + G \varepsilon_{ij} \varepsilon_{ji} + G \ell^2 \partial_k \varepsilon_{ij} \partial_k \varepsilon_{ji} + G \ell'_k \partial_k (\varepsilon_{ij} \varepsilon_{ji}) \tag{17}$$

where $\lambda = E\nu/(1 - 2\nu)(1 + \nu)$ and $G = E/2(1 + \nu)$ are the standard constants of Lamé, E , ν denote the Young's modulus and Poisson's ratio, and as was mentioned already, ℓ , ℓ' are additional characteristic lengths of the material, where

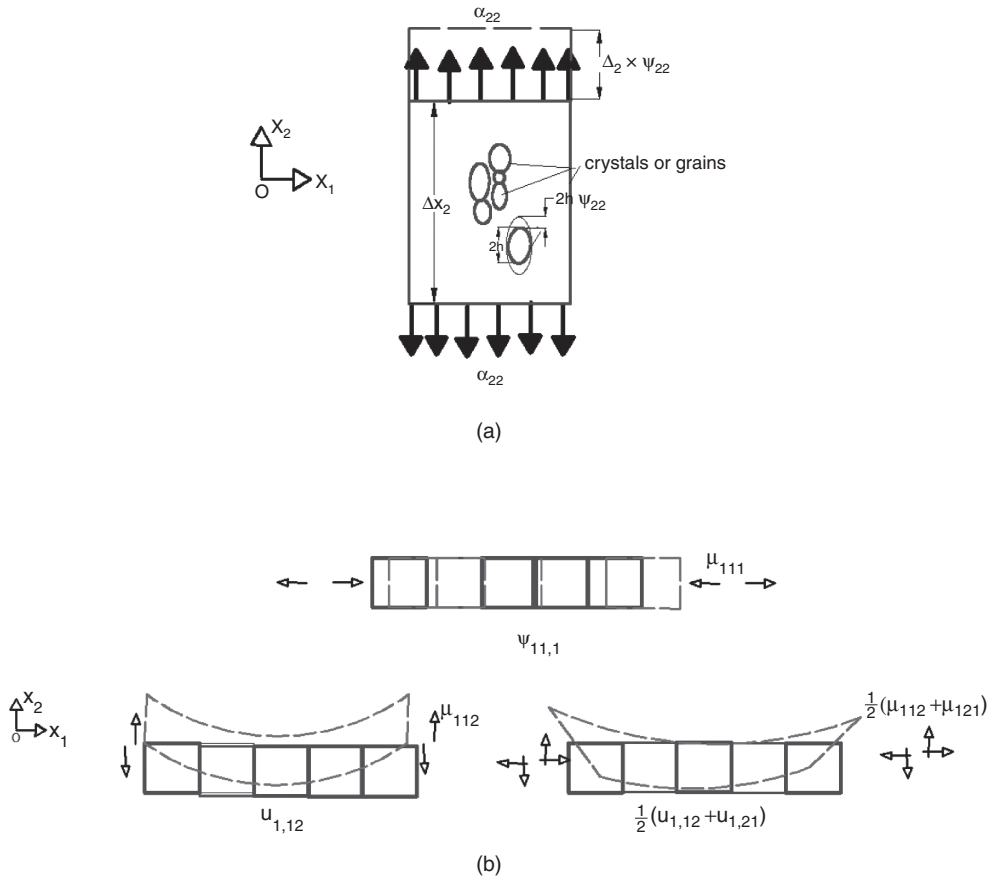


Figure 3 (a) Typical components of relative stress α_{ij} ($\alpha_{ij} \equiv \sigma_{ij} - \tau_{ij}$) displacement gradient ∂u_j , and micro-deformation ψ_{ij} for the simple case of uniaxial tension of a flat plate, and (b) various forms of micro-deformation gradients and associated double stresses.

$$l_k = l' \nu_k, \quad \nu_k \nu_k = 1 \tag{18}$$

is a director. The last term in Equation 17 has the meaning of surface energy, since by using the divergence theorem we get

$$\int_V \partial_r (l_r \varepsilon_{pq} \varepsilon_{qp}) dV = l' \int_{\partial V} (\varepsilon_{pq} \varepsilon_{qp}) (\nu_r n_r) dS \tag{19}$$

wherein n_k is the outward unit normal on the boundary ∂V .

1.3 Stress equations of equilibrium

Germain (1973a, b) suggested a general framework for the foundation of consistent higher grade continuum theories on the basis of the virtual work principle. This

approach starts from the definition of the variation of the total potential energy in a volume V of the body with arbitrary variation of the macro-strain ε_{ij} . A restricted Mindlin continuum, is a micro-homogeneous material for which the macroscopic strain coincides with the micro-deformation, $\gamma_{qr} = 0$ which in turn leads to the following relations

$$\psi_{qr} \equiv \partial_q u_r, \quad \hat{\kappa}_{qrs} \equiv \partial_q \varepsilon_{rs} = (1/2)(\partial_q \partial_r u_s + \partial_q \partial_k u_r) = \hat{\kappa}_{qsr} \quad (20)$$

and

$$\mu_{qrs} \equiv \partial v / \partial \hat{\kappa}_{qrs} = \mu_{qsr} \quad (21)$$

In the particular case the variation of the strain energy potential is defined as follows (Mindlin, 1964)

$$\delta \int_V v dV = \int_V (\tau_{ij} \delta \varepsilon_{ij} + \mu_{ijk} \partial_i \delta \varepsilon_{jk}) dV \quad (22)$$

where

$$\tau_{ij} = \frac{\partial v}{\partial \varepsilon_{ij}}, \quad \mu_{ijk} = \frac{\partial v}{\partial (\partial_i \varepsilon_{jk})} \quad (23)$$

The second order stress tensor τ_{ij} , is dual in energy to the macroscopic strain and is symmetric (*i.e.* $\tau_{ij} = \tau_{ji}$), whereas the third order stress tensor μ_{ijk} , is dual in energy to the strain-gradient. To prepare for the formulation of a variational principle, we apply the chain rule of differentiation and the divergence theorem; furthermore, we resolve $\partial_i u_j$ on the boundary ∂V of V into a plane – gradient and a normal-gradient as follows

$$\partial_i \delta u_j \equiv D_i \delta u_j + n_i D \delta u_j, \quad D_i \equiv (\delta_{ik} - n_i n_k) \partial_k, \quad D \equiv n_k \partial_k, \quad (24)$$

where δ_{ij} is the Kronecker delta. The final expression for the variation in potential energy of a smooth boundary ∂V reads

$$\begin{aligned} \delta U = \int_V \delta v dV = & - \int_V \partial_j (\tau_{jk} - \partial_i \mu_{ijk}) \delta u_k dV + \int_{\partial V} n_j (\tau_{jk} - \partial_i \mu_{ijk}) \delta u_k dS \\ & + \int_{\partial V} \left(\left[\frac{1}{R_1} + \frac{1}{R_2} \right] n_j - D_j \right) n_i \mu_{ijk} \delta u_k dS + \int_{\partial V} n_i n_j \mu_{ijk} D \delta u_k dS \end{aligned} \quad (25)$$

where $(1/R_1 + 1/R_2)$ is the mean curvature of the bounding surface. Looking at the structure of Equation 25 we now postulate the following form for the variation of work U_e done by external forces

$$\delta U_e = \int_V f_k \delta u_k dV + \int_{\partial V} (\tilde{P}_k \delta u_k + \tilde{R}_k D \delta u_k) dS \quad (26)$$

where f_k is the body force per unit volume, \tilde{P}_k , \tilde{R}_k are the specified tractions and double tractions, respectively, on the smooth surface ∂V . Then, from the variational principle, the stress-equilibrium equations in the volume V is found in the following manner

$$\partial_i(\tau_{ij} - \partial_k \mu_{ijk}) + f_j = 0 \tag{27}$$

The workless second order relative stress tensor α_{ij} in a restricted Mindlin continuum is in equilibrium with the double stress (Mindlin, 1964)

$$\alpha_{jk} + \partial_i \mu_{ijk} = 0 \tag{28}$$

Next, by defining the ‘total stress tensor’ σ_{ij}

$$\sigma_{ij} = \tau_{ij} + \alpha_{ij} = \tau_{ij} - \partial_k \mu_{ijk} \tag{29}$$

the stress-equilibrium Equation 27 takes the following final form in the volume V

$$\partial_j \sigma_{ij} + f_i = 0 \tag{30}$$

One may notice that according to Equation 30 the *total stress tensor* is identified with the common (macroscopic) equilibrium stress tensor. Although the above results are obtained for static cases, there is no essential difficulty to derive their dynamic counterpart.

1.4 Boundary conditions

The surface ∂V of the considered volume V is divided into two complementary parts ∂V_u and ∂V_σ such that on ∂V_u kinematic data whereas on ∂V_σ static data are prescribed. In classical continua these are constraints on displacements and tractions, respectively. For the stresses the following set of boundary conditions on a smooth surface ∂V_σ is also derived from the virtual work principle (Wu, 1992; Exadaktylos & Vardoulakis, 2001a)

$$n_j \tau_{jk} - n_j \partial_i \mu_{ijk} + \left(\left[\frac{1}{R_1} + \frac{1}{R_2} \right] n_j - D_j \right) n_i \mu_{ijk} = \tilde{P}_k \tag{31}$$

$$n_i n_j \mu_{ijk} = \tilde{R}_k \tag{32}$$

Since second-grade or grade-2 models introduce second strain gradients into the constitutive description, additional kinematic data must be prescribed on ∂V_u . With the displacement already given in ∂V_u , only its normal derivative with respect to that boundary is unrestricted. This means that on ∂V_u the normal derivative of the displacement should also be given, *i.e.*

$$u_i = w_i \text{ on } \partial V_{u1} \quad \text{and} \quad Du_i = r_i \quad \text{on } \partial V_{u2} \tag{33}$$

1.4 Constitutive relations

From Equations 17 and 23 follow the constitutive relations for the total stress, Cauchy stress and double stress tensors, respectively

$$\left. \begin{aligned} \sigma_{ij} &= \lambda \delta_{ij} \varepsilon_{kk} + 2G(\varepsilon_{ij} - \ell^2 \nabla^2 \varepsilon_{ij}) \\ \tau_{ij} &= \lambda \delta_{ij} \varepsilon_{kk} + 2G \varepsilon_{ij} + 2G \ell_k \partial_k \varepsilon_{ij} \\ \mu_{kij} &= 2G \ell_k \varepsilon_{ij} + 2G \ell^2 \partial_k \varepsilon_{ij} \end{aligned} \right\} \quad (34)$$

From the last of the above relations we may note that the double stress is symmetric in the last two indices as is also depicted by Equation 21.

In closing this exposition of basic notions and relations, we may prove that positive definiteness of the strain-energy density is valid provided the following restrictions of the material constants hold true

$$(3\lambda + 2G) > 0, \quad G > 0, \quad \ell^2 > 0, \quad -1 < \frac{\ell'}{\ell} < 1 \quad (35)$$

The third inequality simply means that ℓ should be a real and not imaginary number.

1.5 Skin effect and surface free energy

Our purpose here is to show that a basic feature of the present strain gradient elasticity theory with surface energy is the appearance of a skin effect associated with the volume energy parameter ℓ . Furthermore, it will be shown that the effect of the relative surface energy parameter ℓ'/ℓ is equivalent to the effect of initial stresses in presence of an infinite, plane boundary.

The deformation of an isotropic semi-infinite body $x_1 \geq 0$ due to a large uniform tensile stress $\sigma_{22} = \sigma$, ($\sigma > 0$), parallel with the surface with outward unit normal vector $(n_1 \ n_2 \ n_3) = (-1 \ 0 \ 0)$ with the Cartesian coordinates be x_1 , x_2 , and x_3 , is considered as was done in (Exadaktylos & Vardoulakis, 1998). Starting from a stress-free configuration, C_0 , the body is stressed uniaxially under plane strain conditions, and C is the resultant configuration. Then, the pre-stressed body is incrementally deformed and let its current configuration state to be that of C' . The problem under consideration is formulated in terms of the first Piola-Kirchhoff stress π_{ij} with respect to current configuration C' , with $\Delta \pi_{ij}$ being its increment referred to the deformed initially stressed state C . Assuming infinitesimal strain elasticity, the Jaumann stress increments $\Delta^\circ \sigma_{ij}$ of the total stress are related directly to the strain increments through constitutive Equations 34. For the traction-free surface of the half-space the following incremental boundary conditions are valid

$$\Delta \pi_{11} = \Delta \pi_{21} = \mu_{111} = \mu_{112} = 0 \quad \text{on } x_1 = 0 \quad (36)$$

It is possible to assume, without loss of generality (it can be shown that, in this problem, the quantities u_1 , u_3 do not couple with u_2 ; these quantities satisfy homogeneous equations with homogeneous boundary conditions and therefore vanish identically) the following displacement field

$$u_2 = u_2(x_1), \quad u_1 = u_3 = 0 \quad (37)$$

and the only non-zero initial stress σ_{22} to act along x_2 -axis. Upon substituting the strain-displacement relation into the stress-strain relations and the resulting expressions for the stresses into the stress-equation of equilibrium $\partial_j \Delta \pi_{ij} = 0$, we find only the following surviving displacement equation of equilibrium

$$\left(1 - \frac{\ell^2}{(1 + \zeta)} \frac{d^2}{dx_1^2}\right) \frac{d^2}{dx_1^2} u_2 = 0 \tag{38}$$

where we have set $\zeta = -\sigma_{22}/2G$. The solution of Equation 38, vanishing at infinity, is

$$u_2(x_1) = c \exp\left(-\frac{\sqrt{1 + \zeta}}{\ell} x_1\right) \tag{39}$$

where c denotes an integration constant. The first three boundary conditions described by Equations 36 are satisfied identically, whereas the only remaining boundary condition along $x_1 = 0$ takes the form

$$\mu_{112} = 2G \left\{ \ell' \frac{d}{dx_1} + \ell^2 \frac{d^2}{dx_1^2} \right\} u_2 = 0 \quad \text{on } x_1 = 0 \tag{40}$$

which holds true for $\nu_r \equiv -n_r$ and gives the following equation

$$c \left[-\frac{\ell'}{\ell} + \sqrt{1 + \zeta} \right] = 0 \tag{41}$$

From Equation 41 one may deduce that the only case which gives non-zero and exponentially decaying displacement with distance from the surface of the solid, that is $c \neq 0$, is the following

$$\frac{\ell'}{\ell} = \sqrt{1 + \zeta} \Leftrightarrow \zeta = - \left[1 - \left(\frac{\ell'}{\ell} \right)^2 \right] \tag{42}$$

The above relation elucidates the importance of the surface strain gradient term ℓ' in determining surface effects. Equation 42 depicts that the effect of the surface energy parameter is equivalent to the effect of an *initial stress*. The dependence of initial stress ζ on the relative surface energy parameter ℓ'/ℓ is shown in Figure 4. From this figure it may be seen that if $\ell'/\ell = 0$ the half-space is under surface tension, with this surface tension to be maximum. As ℓ'/ℓ increases from the value of zero the initial tension or in other words the *surface tension* of the medium decreases reaching the value of zero for $\ell'/\ell = 1$. At $\ell'/\ell = 1$ the initial stress changes sign and for $\ell'/\ell > 1$ becomes compressive in nature. That is, for values of the relative surface energy parameter higher than the value of one, the medium is under surface compression and it is no longer in a state of elastic equilibrium, or in other words as it is also shown by the inequality of Equation 35 its strain energy density function is negative definite.

The elastic strain energy density of the considered 1D configuration is given by

$$v = G \left\{ \varepsilon^2 + \ell^2 \nabla \varepsilon \nabla \varepsilon + 2\ell' \varepsilon \nabla \varepsilon \right\}, \quad \nabla \equiv d/dx_1 \tag{43}$$

Substituting in Equation 43 the values for the strain and the strain-gradient, we find

$$\hat{v} = \left\{ 1 - \left(\frac{\ell'}{\ell} \right)^2 \right\} \left(\frac{\ell'}{\ell} \right)^2 \left(\frac{c}{\ell} \right)^2 \exp\left(-2\frac{\sqrt{1 + \zeta}}{\ell} x_1\right), \quad \hat{v} = v/G \tag{44}$$

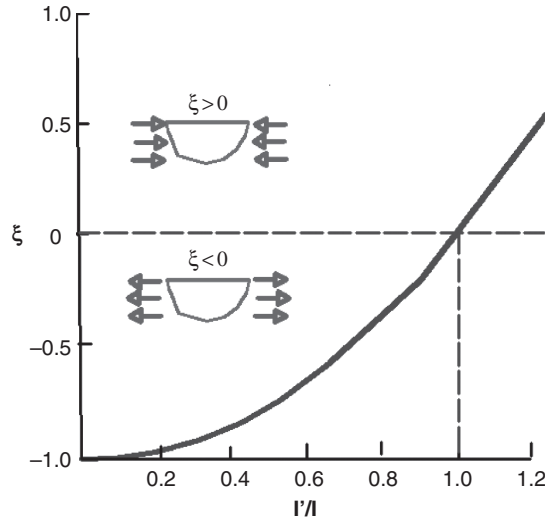


Figure 4 Graphical representation of the relation of the dimensionless pre-stress ξ with the relative surface energy parameter ℓ'/ℓ (Exadaktylos & Vardoulakis, 1998).

By adopting the following definition for the average surface stress (or surface free energy)

$$\gamma_{se} = \int_V v dV / A \tag{45}$$

where A is the area of the free surface, we may find after some manipulations

$$\gamma_{se} = \frac{G}{2} \left\{ 1 - \left(\frac{\ell'}{\ell} \right)^2 \right\} \frac{\ell' c^2}{\ell^2} \tag{46}$$

This is also, for each surface, the energy per unit area required to separate the body along a plane and $\gamma_{se} > 0$ if inequality described by the last of Equations 35 holds true.

1.6 Anti-plane shear (SH) surface waves

There are a number of cases in Rock Mechanics where stresses and strains are of dynamic nature – as in the case of earthquakes, rock blasting and rock bursting - and the propagation of these stresses and strains through the rock mass should be studied (Jaeger *et al.*, 2007). In this context the propagation and interaction of elastic waves with interfaces in the rock mass (like joints, interfaces of geological layers etc) are important. When an incident wave is a shear wave whose displacement vector is parallel to the interface then there are produced anti-plane shear or SH waves since for the case of an interface that is horizontal these waves are polarized in the horizontal plane (Jaeger *et al.*, 2007).

In the next we consider *SH* motions in a gradient elastic half-space with surface energy. With respect to a fixed Cartesian coordinate system $Oxyz$, the half-space occupies the region $(-\infty < x < \infty, y \geq 0)$ and is thick enough in the z -direction to allow an anti-plane shear state when the loading acts in the same direction. In this case and assuming additionally a time-harmonic *steady state*, any problem can be described by the displacement field $u_x = u_y = 0, u_z \equiv w(x, y, t) = w(x, y) \cdot \exp(-i \omega t) \neq 0$, with $i \equiv (-1)^{1/2}$ is the unit imaginary number and ω being the frequency. In the case of *SH* waves, the only surviving equations of motion are one written for the total stresses $(\sigma_{xz}, \sigma_{yz})$ that are given by the constitutive Equations 34a and two written for the double stresses $(\mu_{xxz}, \mu_{xyz}, \mu_{yxz}, \mu_{yyz})$ that are given by constitutive Equations 34c. Vardoulakis & Georgiadis (1997) have shown that the field equation for such a state in terms of displacements is

$$\ell^2 \nabla^4 w - g \nabla^2 w - k^2 w = 0, \tag{47}$$

where ∇^2 and ∇^4 are the Laplace and biharmonic operators, $g = 1 - (\omega^2 \hat{I}/G)$, $k = \omega/V$, $V = (G/\rho)^{1/2}$ is the shear wave velocity in the absence of gradient effects, $\hat{I} = (1/3)\rho b^2$ is the micro-inertia coefficient, ρ is the mass density, and b is the half-length of the crystal (e.g. Figure 3a). Further, operating with the two-sided Laplace transform on Equation 47 yields an o.d.e. for the transformed displacement $w^*(p, y)$. The general solution of the latter equation that is bounded at infinity is

$$\begin{aligned} w^*(p, y) &= B(p) \cdot \exp(-\beta y) + C(p) \cdot \exp(-\gamma y); \\ \beta(p) \equiv \beta &= i(p^2 + \sigma^2)^{1/2}, \quad \gamma(p) \equiv \gamma = (\tau^2 - p^2)^{1/2}, \\ \sigma &= \sqrt{\frac{\sqrt{g^2 + 4\ell^2 k^2} - g}{2\ell^2}}, \quad \tau = \sqrt{\frac{\sqrt{g^2 + 4\ell^2 k^2} + g}{2\ell^2}}, \end{aligned} \tag{48}$$

where p is the Laplace-transform variable and B, C are obtainable through enforcement of the boundary conditions.

As is well known, the criterion for *surface waves* is that the displacement decays exponentially with distance from the free surface (Achenbach, 1973). Thus, if we consider *plane-wave* solutions of the form $\exp[i(qx - \omega t)]$ with a dispersion relation $\omega = \omega(q)$, a distinct harmonic component of propagation of the *SH* surface wave satisfying the equations for a grade-2 continuum in the half-space $y \geq 0$ will be expressed as

$$\begin{aligned} \bar{w}_s(x, y, t) &= [B(q) \cdot \exp(-|\beta|y) + C(q) \cdot \exp(-|\gamma|y)] \cdot \exp[iq(x - C_{pb}t)] \\ C_{pb} &= \frac{\omega}{q}, \end{aligned} \tag{49}$$

where C_{pb} is the phase velocity, $q \equiv (p/i)$ is the wave number which should be a real quantity such that $-\infty < q < -\sigma$ or $\sigma < q < \infty$ in order for surface waves to exist, $|\beta| = (q^2 - \sigma^2)^{1/2}$ and $|\gamma| = (q^2 + \tau^2)^{1/2}$. Next, the appropriate *dispersion* (or *frequency*) *equation* can be obtained by enforcing the pertinent boundary conditions at the half-space surface. These are zero traction conditions which in the transform domain provide a linear homogeneous system. This has a nontrivial solution if and only if

$$\begin{aligned}
 & -(\sigma_d^2(q_d^2 - \sigma_d^2)^{1/2} + \tau_d^2(q_d^2 + \tau_d^2)^{1/2}) + m\alpha_d^2 = 0, \sigma_d < |q_d| < \infty; \\
 & q_d = \ell q, \sigma_d = \ell \sigma, \tau_d = \ell \tau, m = \ell' / \ell, \alpha_d^2 = \ell^2 \alpha^2 = (g^2 + 4\ell^2 k^2)^{1/2}.
 \end{aligned} \tag{50}$$

Equation 50 constitutes the dispersion relation for surface waves. Since this is an irrational algebraic equation, a single mode of SH waves may exist that is directly related to the parameter m . Another immediate observation is that SH surface waves do exist only when $\ell \neq 0$ and $m > 0$. This finding means that the inclusion of the surface energy strain gradient term ℓ' , that expresses an *anisotropy in the microscale*, is necessary for predicting surface SH waves. In order to obtain numerical results for the relation between the phase velocity C_{pb} and the wavenumber q (or, equivalently, the wavelength $\lambda = 2\pi/q$), one has generally to *numerically* solve Equation 50. Here, however, we chose to work in a different manner and obtain some representative *exact* results, which can be obtained for the particular case $\ell = (1/\sqrt{3})b$. The latter is equivalent to the relation $\omega_d^2 = \ell^2 k^2$. Then, Equation 50 takes the form

$$-\omega_d^2 \sqrt{q_d^2 - \omega_d^2} - \sqrt{q_d^2 + 1} + m(1 + \omega_d^2) = 0, \tag{51}$$

where $\omega_d^2 = 1 - g$. Further, the above irrational equation possesses four roots, three of which are extraneous and, therefore, possess no physical meaning. Also, the appearance of complex roots marks cut-off frequencies. It can be shown that the following root is the only one satisfying the original Equation 51,

$$q_d = \begin{cases} \frac{\sqrt{\omega_d^6 - 2\omega_d^4 + 2\omega_d^2 - 1 + m^2(1 + \omega_d^4)} - 2m\omega_d^2 \sqrt{\omega_d^2 + (m^2 - 1)}}{|1 - \omega_d^2|}, & \omega_d \neq 1 \\ \frac{1}{2} \frac{\sqrt{1 + 4m^4}}{m}, & \omega_d = 1 \end{cases} \tag{52}$$

For high frequencies the first of the Equation 52 assumes the asymptotic expansion $q_d = \omega_d + (1/2)m^2(\omega_d^{-1}) + O(\omega_d^{-2})$; $\omega_d \rightarrow \infty$, whereas the following relations are generally valid for the particular case $\ell = (1/\sqrt{3})b$

$$\frac{C_{pb}}{V} = \frac{\omega_d}{q_d}, \quad \frac{\lambda}{b} = \frac{2\pi}{\sqrt{3}} \frac{1}{q_d} \tag{53}$$

and facilitate the creation of the graphs illustrated in Figure 5. From these curves it can be seen that there is a minimum velocity. We also note that the graphical form of the dispersion relation reminds the one found by Coulson (1958) for surface waves in liquids that possess *surface tension*.

1.7 Rayleigh waves in grade-2 elastic solids

The possibility of a wave traveling along the free surface of an elastic half-space, under conditions of plane stress or plane strain, such that the disturbance is largely confined to the neighborhood of the boundary was first considered by Lord Rayleigh (1887). The classical theory of linear elasticity does not predict any dispersion for these motions;

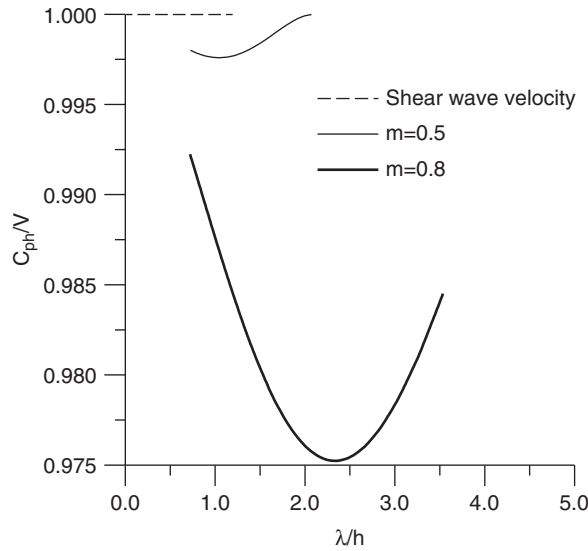


Figure 5 Dispersion curves for the propagation of SH surface waves showing the variation of the normalized phase velocity C_{ph}/V with the normalized wavelength λ/h .

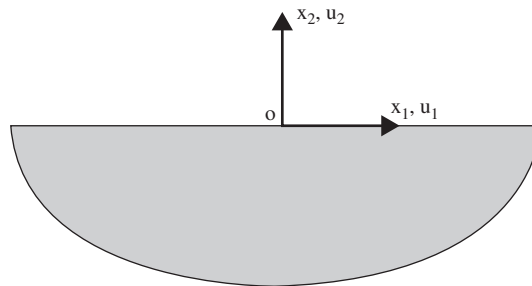


Figure 6 Half-space and coordinates.

only by including *viscoelastic* (Currie *et al.*, 1977) or *thermoelastic* (Georgiadis *et al.*, 1998) effects in the constitutive behavior leads to *dispersive* Rayleigh waves. In order to explain the occurrence of dispersion of Rayleigh waves, Vardoulakis (1981) has considered a graded half-space, that is a material with stiffness increasing with depth. Here, we take another point of view and consider the propagation of Rayleigh waves in a *gradient-elastic, macrohomogeneous and isotropic* half-space $x_2 \geq 0$ (Figure 6) having as an objective examining the possibility of dispersive behavior.

In particular, the theory utilized here can be considered one of the simplest versions of Mindlin's theory containing only the volumetric length scale corresponding to the following strain-energy density function

$$v = (1/2)\lambda \varepsilon_{qq} \varepsilon_{rr} + G \varepsilon_{qr} \varepsilon_{rq} + G \ell^2 (\partial_s \varepsilon_{qr}) (\partial_s \varepsilon_{rq}) \tag{54}$$

The displacement equation of motion in the absence of body force may be derived in the following manner

$$G\bar{D}^2 \nabla^2 \mathbf{u} + (\lambda + G\bar{D}^2) \nabla \nabla \cdot \mathbf{u} = \rho \ddot{\mathbf{u}} - \frac{1}{3} \rho b^2 \nabla^2 \ddot{\mathbf{u}} \tag{55}$$

where we have used the operator $\bar{D}^2 \equiv 1 - \ell^2 \nabla^2$. The boundary conditions for the problem at hand, for $h/\ell \rightarrow 0$ and for the two cases of boundary conditions (Case I refers to the approximate and II to the exact boundary conditions, respectively) take the form

$$\begin{aligned} \sigma_{22} = \sigma_{21} = 0 \quad (\text{Case I}) \\ \sigma_{22} - \frac{\partial \mu_{221}}{\partial x_1} = 0, \quad \sigma_{21} - \frac{\partial \mu_{211}}{\partial x_1} = 0 \quad (\text{Case II}), \\ \mu_{222} = \mu_{221} = 0 \quad (\text{Case I, II}), \quad -\infty < x_1 < \infty, \quad x_2 = 0 \end{aligned} \tag{56}$$

Then we fix the wave numbers, as well as Poisson’s ratio, and we construct the equation for the characteristic determinant of the problem at hand as an equation for the dimensionless frequency $\Omega = \omega \ell / c_T$ (Stavropoulou *et al.*, 2003). It is not difficult to verify that for $\ell = 0$, the determinant equation reduces to the classical Rayleigh function whose roots are given by Eringen & Suhubi (1975) for various Poisson’s ratios ν . It is also clear that the root of the determinant equation is a function of ℓ , consequently in contrast to the classical theory the Rayleigh wave velocity predicted by the proposed gradient elasticity theory is dispersive. Figure 7 illustrates the relation exhibited between the normalized phase velocity of Rayleigh wave with the normalized frequency in the framework of the present theory for the case of rock with small grain size, *i.e.* $h/\ell \ll 1$.

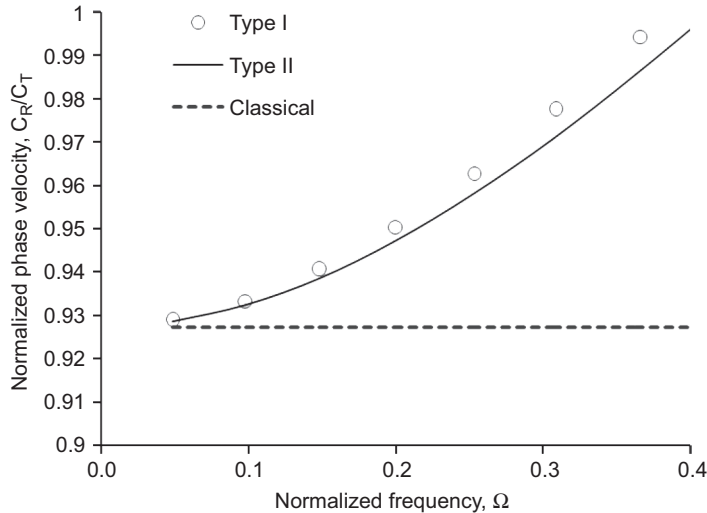


Figure 7 Dispersion curve for the propagation of Rayleigh surface waves showing the variation of the normalized phase velocity with the normalized frequency for h/ℓ tending to zero and $\nu = 0.3$ (Stavropoulou *et al.*, 2003).

The following conclusions can be drawn from the analysis given above:

- If the volumetric gradient length scale ℓ is small compared to the characteristic wavelength of the Rayleigh wave then the results obtained from gradient and classical elasticity theories coincide.
- For increasing relative frequencies the gradient theory predicts larger Rayleigh wave velocities than the classical theory in a monotonic manner. This property - which is due to the fact that $b/\ell \ll 1$ - may be used to establish the gradient parameter ℓ through carefully performed Rayleigh wave propagation experiments. This has been demonstrated with the analysis of Rayleigh wave experiments in Pentelikon marble used for the construction of Parthenon monument in Athens (Stavropoulou *et al.*, 2003).
- A new material parameter may be defined as the product $G\ell$ with dimensions of $[FL^{-1}]$, where F denotes force and L denotes length. This new parameter is called ‘crack stiffness’ and influences the magnitude of mode-I, -II and -III crack deformation under given stress in rocks. It was demonstrated (Stavropoulou *et al.*, 2003) that this parameter may be experimentally determined through carefully performed in situ Rayleigh wave measurements.
- The results obtained by applying the two types of boundary conditions do not differ appreciably in the whole range of normalized frequencies of Rayleigh waves.

1.8 Size effect of the fracture toughness of the pressurized crack

The possible size effect exhibited by hydraulic fractures – *i.e.* the dependence of the resistance of fracture to propagation with increasing crack length – is a very important problem in hydraulic fracturing of rocks. Exadaktylos (1998) has postulated the following criterion for mode-I fracture propagation subjected to constant internal pressure (assuming zero diffusivity of the rock)

$$\Psi(\alpha - \eta; \sigma_0, \ell, \ell') \geq \beta, \quad \Psi(\alpha - \eta; \ell, \ell') = \frac{\pi\alpha\sigma_0^2}{8G} \hat{\psi}(\alpha - \eta) = \frac{K_I^2}{8G} \hat{\psi}(\alpha - \eta) \quad (57)$$

where the function Ψ depends on the applied pressure on the crack lips σ_0 , and the two strain gradient length scales. The quantity β has the dimensions of specific volume energy or stress $[FL^{-2}]$, that was called ‘modulus of cohesion’ and is assumed to be a constant material parameter. The symbol η is a small length with respect to the semi-crack length α , in order to remove the weak logarithmic singularity of the function $\hat{\psi}(t)$ at $t = \alpha$; the latter function is given in closed form. This criterion was applied after the solution of the relevant boundary value problem in the frame of grade-2 Casal-Mindlin theory. This solution revealed that the crack shape is no longer elliptical as is predicted by the classical theory but the crack lips take a cusp shape such as shown in Figure 8a.

By setting $K_I = K_{IC}$ in the above criterion of Equation 57 we obtain the following expression for the fracture toughness

$$K_{IC} = \sqrt{\frac{8\beta G}{\hat{\psi}(\alpha - \eta)}} \quad (58)$$

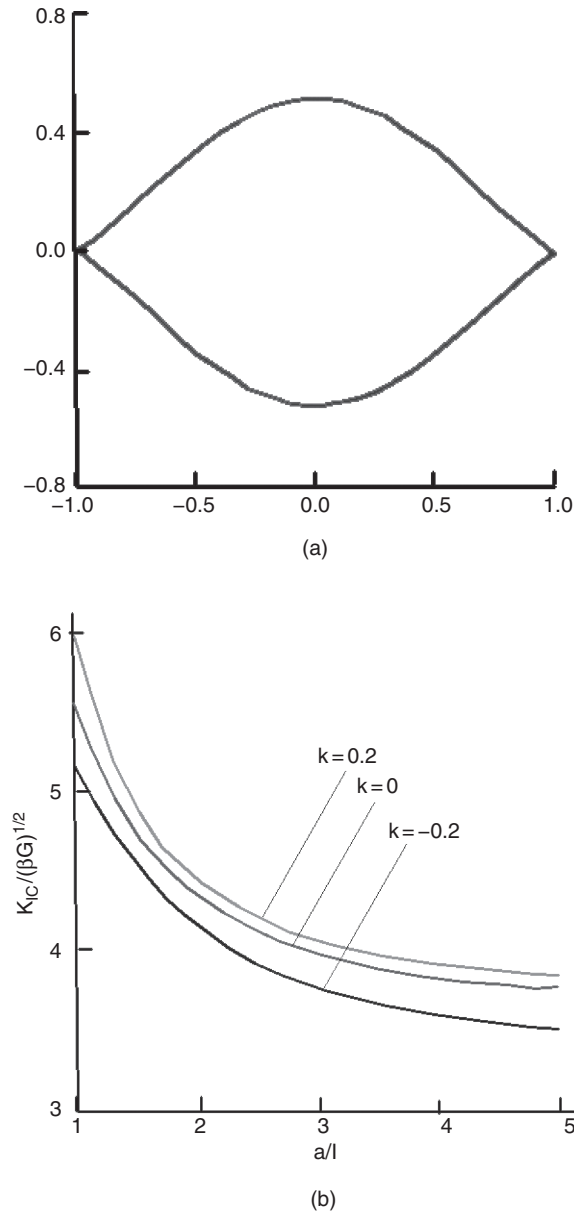


Figure 8 (a) Deformed mode-I crack with tips in the form of cusps of first kind, and (b) size effect of the normalized mode-I fracture toughness K_{IC} for three values of the material length ratio $k = \ell'/\ell$ and for Poisson's ratio of the material $\nu = 1/4$ (Exadaktylos, 1998).

The size-effect of the fracture toughness is demonstrated in Figure 8b for the various values of the relative surface energy parameter $k = \ell'/\ell$. It may be observed that: (a) that as the surface energy length scale increases the fracture toughness increases due to the surface tension effect mentioned in Paragraph 1.5 above, and (b) the size

effect resembles that of the simple stress-mean-value theory presented in Paragraph 1.1 (e.g. Figure 2).

2 A GRADE-2 ENGINEERING BEAM THEORY WITH SURFACE ENERGY

2.1 Introductory remarks

The experimental analysis for mechanical parameters identification like modulus of elasticity and tensile strength of rocks and other brittle structural materials, as well as theoretical models of the deformability and strength of beams, beams-columns and plates, are of great practical interest in many applications in rock and structural engineering. They depict the serviceability and strength of such types of engineering structures. Beam elements occupy a wide range of technological applications and length scales. For example, in Civil Engineering applications beams from timber, steel, concrete, aluminum etc are used as structural elements in buildings and bridges, at the scale of several meters to several tenths of meters. In Monumental Constructions and restoration works one may mention *marble or limestone beams* in temples resting on marble columns with spans of the order of several meters. In Mining and Tunneling one may encounter artificial span support beams (from timber, cast iron, concrete etc) or beams and plates overhanging above underground openings in mines, tunnels and caverns. For example a beam may be formed by a rock layer at tunnel's roof with one end free (entrance) and the other hinged (tunnel's face). Beams are also encountered in biomechanical applications: e.g. micro-cantilever sensors at the scale of $1\div 10\ \mu\text{m}$, and in nanomechanical applications in thin films technology, biosensors and atomic force microscopes at the scale of $10\div 100\ \text{nm}$. For this purpose, there is a growing interest of proper theories incorporating additional to the characteristic macroscale also smaller length scales (these are called micromechanical theories and they include discrete and distinct element theories among others).

Here, Timoshenko's engineering beam bending theory of linear elastic materials is extended by considering surface energy effects that have been discussed in Section 1. A beam bending micromechanical theory with surface energy is formulated that is based on a modified strain energy function of a material with microstructure that includes the classical Bernoulli-Euler term, the shape correction length scale ℓ_v introduced by Timoshenko to account for the effect of shear forces, and another extra new length scale ℓ_s introduced here, that is associated with surface energy effects.

2.2 Fundamentals of the technical beam theory

The longitudinal section of the beam is referred to a Cartesian coordinate system $O(x, y, z)$ positioned on the neutral axis – which is the locus of centroids of cross-sections - with its origin at mid-span and with the Ox -axis directed along the neutral axis of the beam while Oz -axis extending vertically downwards. Deformation quantities are assumed as infinitesimal, and the corresponding displacements of points in a cross-section along Ox and Oz directions are denoted by the symbols u, w respectively. Let the infinitesimal normal strains $\varepsilon_{xx}, \varepsilon_{zz}$ and the engineering shear strain γ_{xz} in the plane xOz to be defined as follows

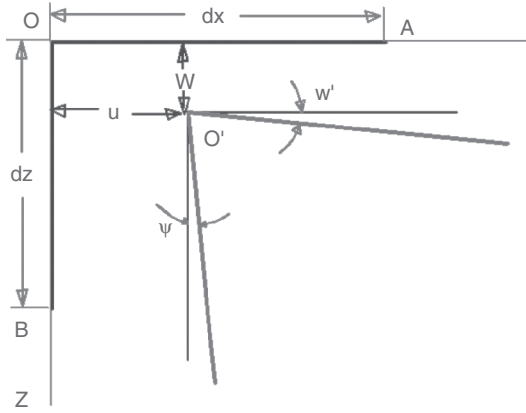


Figure 9 Deformations of vertical and horizontal beam sections.

$$\varepsilon_{xx} = \varepsilon = u_{,x}, \quad \varepsilon_{zz} = w_{,z}, \quad \gamma_{xz} = \gamma = u_{,z} + w'_{,x} \quad (59)$$

where ψ denotes the rotation (considered to be a small quantity) of the cross-section A of the beam at position x (Figure 9) and the comma denotes differentiation w.r.t. the variable after the comma. It may be easily shown that the representation of the strain energy density (potential) of the beam in the context of Timoshenko's beam bending theory is given by the following *ansatz*

$$v_T = \frac{1}{2} EI \left(\kappa^2 + \frac{\gamma^2}{l_v^2} \right) \quad (60)$$

where the term EI denotes the flexural rigidity or stiffness of the beam, I denotes the moment of inertia of the cross-section A of the beam, l_v stands for a microstructural length scale of the beam material that considers the effect of the transverse shear stress contributing to the deflection $w = w(x)$ of the beam, the symbol κ we denote the gradient of the rotation angle (bending curvature) of the cross-section, that is

$$\kappa \equiv \psi_{,x} \quad (61)$$

In the frame of this technical theory the horizontal strain is simplified as follows

$$\varepsilon = \kappa z \quad (62)$$

Also, the bending curvature $\kappa = 1/R$ is found as $\partial\varepsilon/\partial z = \psi_{,x}$.

The following constitutive relationships for the bending moment and transverse shear force may be deduced

$$M = \frac{\partial v_T}{\partial \kappa} = EI\kappa, \quad Q = \frac{\partial v_T}{\partial \gamma} = EI \frac{\gamma}{l_v^2} \quad (63)$$

where the shear forces and bending moments, are denoted as Q , M , respectively, The first of Equations 63 forms the Bernoulli-Euler theorem depicting the analogy of the bending moment with the bending curvature of the beam, while the second is due to

Timoshenko that considers the effect of the transverse shear forces on the beam deflection. The characteristic length scale ℓ_v is related to the dimensionless quantity ℓ_T in the following manner

$$\ell_v^2 = (\ell_T L)^2 \tag{64}$$

For example for a rectangular cross-section with height H , we get that ℓ_T essentially compares with the inverse of the aperture ratio of the beam, that is to say for a rectangular cross-section of the beam, Timoshenko (1921) found that ℓ_T compares with the inverse of the length to height ratio

$$\ell_T^2 = \frac{1}{5}(1 + \nu) \left(\frac{H}{L}\right)^2 \ll 1 \quad \text{for } H < L \tag{65}$$

Accordingly for long prismatic beams ($\ell_T \ll 1$) or ($H/L \ll 1$) Bernoulli-Euler elementary beam theory is recovered.

2.3 Formulation of the kappa-gamma beam technical theory

Herein an engineering beam bending theory that has been previously presented by Vardoulakis *et al.* (1998) containing two material length scales and aiming at capturing the size effect exhibited by beams in bending, is reformulated. In fact we change the strain energy density (or elastic potential energy density) *ansatz* for an elastic material with microstructure initially proposed in our previous work, with the following straightforward expression

$$v_E = \frac{1}{2}EI \left(\kappa^2 + \frac{1}{\ell_v^2} \gamma^2 + \frac{2}{\ell_s} \kappa \gamma \right) \tag{66}$$

So, Bernoulli-Euler theory which leads to the proportionality of the bending moment with curvature kappa (κ), is expressed only by the first term, whereas Timoshenko’s beam bending theory that explains the effect of shear forces (gamma) on beam deflection and bending curvature of the beam is expressed by the first two terms. The third term in the above strain energy density function has not been obtained arbitrarily, but rather on the simple and straightforward argument, namely that since the curvature and shear strain are already included by Bernoulli-Euler and Timoshenko, respectively, then their product should be also included for completeness of the representation. This argument introduces an additional material length scale ℓ_s . It may be easily shown that the positive-definiteness of the strain energy density is guaranteed if the following inequalities are valid

$$-1 < \frac{\ell_v}{\ell_s} < 1 \tag{67}$$

wherein from Equations 64 & 65

$$\ell_v^2 = (\ell_T L)^2 = \frac{1}{5}(1 + \nu)H^2 \tag{68}$$

that is, for positive strain energy density Timoshenko’s shape factor ℓ_v must not vanish if surface or scale effects are going to be taken into account. The above *ansatz* described

by Equation 66 contains the last term that considers surface energy effects through the microstructural length scale ℓ_s , and also contains as a special case Timoshenko's beam bending theory through the length scale ℓ_v , as may be observed from Equation 60. In fact, by applying Gauss' divergence theorem the total elastic strain energy of the beam takes the form

$$\begin{aligned}
 U_E &= \frac{1}{2} EI \int_0^L \left(\kappa^2 + \frac{1}{\ell_v^2} \gamma^2 + \frac{2}{\ell_s} \kappa \gamma \right) dx \\
 &= \frac{1}{2} EI \int_0^L \left(\kappa^2 + \frac{1}{\ell_v^2} \gamma^2 + \frac{2}{\ell_s} \kappa w' \right) dx + \frac{1}{2\ell_s} EI \int_0^L \nabla \psi^2 dx \\
 &= \frac{1}{2} EI \int_0^L \left(\kappa^2 + \frac{1}{\ell_v^2} \gamma^2 + \frac{2}{\ell_s} \kappa w' \right) dx + \frac{1}{2\ell_s} EI [\psi^2]_0^L
 \end{aligned} \tag{69}$$

where we have set $(\cdot)' \equiv \nabla(\cdot) \equiv d/dx$. The constitutive equations for the shear force Q and bending moment M , are also easily derived from the potential of Equation 66 as follows

$$Q \equiv \frac{\partial v_E}{\partial \gamma} = EI \left(\frac{1}{\ell_v^2} \gamma + \frac{1}{\ell_s} \kappa \right) = EI \left(\frac{1}{\ell_v^2} [w' + \psi] + \frac{1}{\ell_s} \psi' \right) \tag{70}$$

$$M \equiv \frac{\partial v_E}{\partial \kappa} = EI \left(\kappa + \frac{1}{\ell_s} \gamma \right) = EI \left(\psi' + \frac{1}{\ell_s} [w' + \psi] \right) \tag{71}$$

Vardoulakis *et al.* (1998) who studied the size effect exhibited by the flexural strength of marble beams in laboratory tests employed the following ansatz

$$v_{VE} = \frac{1}{2} EI [\kappa^2 + \ell_v^2 (\nabla \kappa)^2 + \ell_s \nabla(\kappa^2)] \tag{72}$$

This is a gradient *almost* B-E theory enhanced with two length-scales where the second term accounts for the shear strain effect

$$\gamma \approx \ell_v^2 \nabla \kappa \tag{73}$$

Papargyri-Beskou *et al.* (2003) assumed only one surviving surface length scale $\ell_x = \ell' \nu_x$ along the axial direction of long beams (very small height to span ratio) according to Casal's theory, and a volumetric length scale denoted in their paper by the symbol g , and made the reasonable assumption of null transverse normal strain $\varepsilon_{zz} = 0$ of the technical beam theory, according to the notation used in the present paper

$$v_{PB} = \frac{1}{2} EI \left[(w'')^2 + g^2 (w''')^2 + 2\ell_x w'' w''' \right], \quad \ell_x \ll 1 \tag{74}$$

Our kappa-gamma model for long beams (*i.e.* B-E theory) such that the following approximations to be valid

$$\kappa = \frac{d\psi}{dx} \approx -\frac{d^2w}{dx^2}, \quad \gamma = \frac{dw}{dx} + \psi \approx -\ell_T^2 \frac{d^3w}{dx^3} \tag{75}$$

gives

$$v_{PB} \approx \frac{1}{2}EI \left[(w'')^2 + \left(\frac{\ell_T^2}{\ell_v}\right)^2 (w''')^2 + \frac{2\ell_T^2}{\ell_s} w'' w''' \right] = v_b, \quad \ell_T^2 \ll 1 \tag{76}$$

that is exactly the same to the elastic potential proposed by Papargyri-Beskou *et al.* (2003).

Later on, Vardoulakis & Giannakopoulos (2006) have proposed the following potential or strain energy density (energy per unit beam length) for the beam

$$v_{VG} = \frac{1}{2}EI \left(\kappa^2 + \frac{1}{\ell_v^2} \gamma^2 + \frac{2}{\ell_s} (\kappa')^2 \right) \tag{77}$$

It may be noted that the first two terms of the kappa-gamma potential have the same form with those appearing in the ansatz given by Equation 77, although they differ in the last term.

2.4 Generalization of the gradient beam theory with surface energy

A general expression of the elastic strain energy density of a gradient elastic solid with surface energy with two additional length scales has been given by Equation 17. Applying the following simplifications

$$\varepsilon_{xx} = \kappa z, \quad \varepsilon_{xz} = \frac{1}{2} \gamma \tag{78}$$

and elaborating on the expressions, the final expression of the strain energy density for the beam is composed from three distinct parts. Firstly, the classical part of the elastic potential energy may be found in the following manner,

$$v^{clas} = \iint_A \left[\left(\frac{1}{2} [\lambda + 2G] z^2 \right) \kappa^2 + \frac{1}{2} G \gamma^2 \right] dA = \frac{1}{2} [\lambda + 2G] I \kappa^2 + \frac{1}{2} G \gamma^2 A, \tag{79}$$

$$I = \iint_A z^2 dA$$

~~where A denotes the cross-sectional area of the beam.~~ This expression is composed from two terms appearing also in the elastic potential energy Equations 66, 72, 76 and 77. Secondly, one may find a volumetric part that is associated with the volumetric length scale which does not give a scale effect, namely

$$v^{vol-grad} = G \ell^2 \iint_A \left[z^2 \left(\frac{\partial \kappa}{\partial x} \right)^2 + \frac{1}{2} (w_{,xx} + \kappa)^2 + \kappa^2 \right] dA \Leftrightarrow \tag{80}$$

$$v^{vol-grad} = G \ell^2 \left[I \left(\frac{\partial \kappa}{\partial x} \right)^2 + \frac{1}{2} A \nabla \gamma \nabla \gamma + A \kappa^2 \right]$$

One may note that the first term of the last expression is the same ~~used~~ by Vardoulakis & Giannakopoulos (2006), and that is why their model does not predict a scale effect. Finally, it may be found a surface energy part associated with the only surviving surface energy length scale $\ell_x = \ell' \nu_x$ that gives a size effect, *i.e.*

$$\begin{aligned}
 v^{surf-grad} &= 2G\ell' \iint_A \left[z^2 \kappa \frac{\partial \kappa}{\partial x} + \frac{1}{2} (\kappa + w_{,xx}) \gamma \right] dA \Leftrightarrow \\
 v^{surf-grad} &= 2G\ell' \left[I\kappa \frac{\partial \kappa}{\partial x} + \frac{A}{2} \kappa \gamma + \frac{A}{2} w_{,xx} \gamma \right]
 \end{aligned} \tag{81}$$

The first term of the expression above $\kappa \nabla \kappa$ has been adopted by Vardoulakis *et al.* (1998), while the second term of the expression above is the third term of the kappa-gamma beam theory. In Vardoulakis *et al.* (1998) and in the present publication it is demonstrated that both technical theories are capable to predict scale effects of beams.

The transverse shear force and bending moment expressions resulting from the 3D gradient theory may be formally derived in the following manner and are equivalent with Equations 70 and 71, respectively,

$$Q = \frac{\partial v^{2ndgr}}{\partial \gamma} = G \left(\gamma + \ell' \kappa + \ell' w_{,xx} \right) \iint_A dA, \tag{82}$$

$$\begin{aligned}
 M = \frac{\partial v^{2ndgr}}{\partial \kappa} &= 2[\lambda + 2G]\kappa \iint_A z^2 dA + G\ell' \gamma \iint_A dA + \\
 &+ G\ell^2 \left(\frac{\partial \gamma}{\partial x} + 2\kappa \right) \iint_A dA + 2G\ell' \frac{\partial \kappa}{\partial x} \iint_A z^2 dA
 \end{aligned} \tag{83}$$

By comparing the above two sets of relationships 82 & 70 it may be observed that the kappa-gamma theory does not contain the kinematical term w_{xx} in the expression for the transverse shear force, and the terms $\partial \gamma / \partial x$, $\partial \kappa / \partial x$ in the expression for the bending moment (*e.g.* compare Equations 83 & 71).

2.5 Closed-form solution of 3PB simply supported beam

Next we proceed with the solution of the 3PB configuration employing the simpler engineering beam theory. It may be shown that the equilibrium equations for the beam

$$\frac{dQ}{dx} = 0, \quad -Q + \frac{dM}{dx} = 0 \tag{84}$$

are automatically satisfied, with the following expressions for the bending moment and transverse shear force along the beam subjected to concentrated loading P at its mid-span (natural boundary condition

$$M = \frac{PL}{4} \left(1 - \frac{2x}{L} \right), \quad Q = -\frac{P}{2} \quad 0 \leq x \leq \frac{L}{2} \tag{85}$$

Substituting the values of Q, M given by the above Equations 85 into Equations 84 the following system of linear odes is obtained

$$\left. \begin{aligned} \ell_r(w' + \psi) + \psi' &= -\lambda, \\ \ell_s \psi' + w' + \psi &= \frac{\lambda L}{4} \left(1 - 2\frac{x}{L}\right), \end{aligned} \right\} \quad 0 \leq x \leq \frac{L}{2} \quad (86)$$

wherein we have set the following normalized variables with units [L⁻¹]

$$\lambda = \frac{Pl_s}{EI}, \quad \ell_r = \frac{\ell_s}{\ell_v^2} \quad (87)$$

The closed form solution of the above system of ode's has as follows

$$\begin{aligned} \psi &= \frac{1}{4(1 - \ell_r \ell_s)} [\lambda(L + 4\ell_s) + 4C_2(\ell_r \ell_s - 1) - \lambda(4 + \ell_r L)x + \lambda \ell_r x^2], \\ w &= \frac{1}{24(\ell_r \ell_s - 1)} [24C_1(\ell_r \ell_s - 1) + 24C_2(\ell_r \ell_s - 1)x - 3\lambda(2 + \ell_r L)x^2 + 2\lambda \ell_r x^3] \\ 0 \leq x &\leq \frac{L}{2} \end{aligned} \quad (88)$$

in which C₁, C₂ are integration constants to be found from appropriate boundary conditions. The *essential boundary conditions* refer to the vertical displacement at the supported end of the beam, as well as the rotation at the mid-span; both of them should vanish, *i.e.*

$$\begin{aligned} w &= 0, \quad x = \frac{L}{2} \\ \psi &= 0, \quad x = 0 \end{aligned} \quad (89)$$

Substituting the deflection from Equation 88₂ and the rotation from Equation 88₁ into the two kinematical conditions described by Equations 89 we may easily obtain the expressions for the two constants in the following manner

$$C_1 = \frac{\lambda L^2}{48} \frac{\left(L\ell_r + 12\frac{\ell_s}{L} + 6\right)}{\eta^2 - 1}, \quad C_2 = 0 \quad (90)$$

where we have set the dimensionless parameter

$$\eta^2 = \ell_r \ell_s = \left(\frac{\ell_s}{\ell_v}\right)^2, \quad \eta^2 > 1 \quad (91)$$

Subsequently, the expression for the deflection may be found from Equation 88₂ and the above expressions for the constants, that is to say

$$\begin{aligned} w &= \frac{w_c}{\eta^2 - 1} \left\{ 6\hat{\ell}_s \left(1 + 2\hat{\ell}_s\right) + \eta^2 - 12\hat{\ell}_s \left(1 + 2\hat{\ell}_s\right) \xi - 6\eta^2 \xi^2 + 4\eta^2 \xi^3 \right\}, \\ 0 \leq \xi &\leq \frac{1}{2} \end{aligned} \quad (92)$$

where we have used the following dimensionless quantity

$$w_c = \frac{PL^3}{48EI} \tag{93}$$

w_c represents the maximum (*i.e.* mid-span) deflection derived from *Bernoulli-Euler* beam theory. Also, the rotation of the initially vertical cross-section of the beam could be found from Equations 85₁ and 90, *i.e.*

$$\psi = \frac{\bar{\lambda}}{\eta^2 - 1} \zeta \left\{ 2\hat{\ell}_s + \eta^2 - \eta^2 \zeta \right\}, \quad 0 \leq \zeta \leq \frac{1}{2} \tag{94}$$

wherein

$$\bar{\lambda} = \frac{PL^2}{4EI}, \quad \hat{\ell}_s = \frac{\ell_s}{L} \tag{95}$$

The engineering shearing strain could be also found in the following manner

$$\gamma = w' + \psi = \frac{\bar{\lambda}}{\eta^2 - 1} \left\{ -\hat{\ell}_s [1 + 2\hat{\ell}_s] + 2\hat{\ell}_s \zeta \right\}, \quad 0 \leq \zeta \leq \frac{1}{2} \tag{96}$$

In addition, the bending curvature of the beam may be found by formal differentiation of Equation 94 as follows

$$\kappa = \frac{\bar{\lambda}}{L} \frac{1}{\eta^2 - 1} \left\{ 2\hat{\ell}_s + \eta^2 - 2\eta^2 \zeta \right\}, \quad 0 \leq \zeta \leq \frac{1}{2} \tag{97}$$

As, it may be seen from Equation 97, in contrast to classical theory, the present gradient theory with surface energy predicts always for any value of η^2 a finite and larger value of the beam curvature at its supporting ends (*i.e.* for $\zeta = 1/2$). This is due to the presence of the surface energy term $2\hat{\ell}_s$ in the expression for the curvature that also is responsible for the inequality $\kappa \neq -\partial^2 w / \partial x^2$.

2.6 Numerical results

Various beam deflection curves obtained from the theory are shown in Figures 10 a÷c. For this purpose use was made of Equation 92 and of the following expression

$$\eta^2 = \left(\frac{\ell_s}{\ell_v} \right)^2 = \frac{5\hat{\ell}_s^2}{(1 + \nu) \left(\frac{H}{L} \right)^2}, \quad \eta^2 > 1 \tag{98}$$

As was expected the gradient theory, *i.e.* for the relative length scale η comparable to unity, predicts always larger beam deflections compared to the classical B-E theory for $\eta \gg 1$. This is clearly illustrated in Figure 10a. According to Equation 98 the latter case is approached for beams of very large span (L) compared to their height (H) and vanishing surface energy length scale. The effect of Poisson’s ratio on beam deflection for vanishing surface energy term and $H/L=1/10$ is displayed in Figure 10b. Finally, the effect of the surface energy length on the beam’s deflection for constant $H/L=1/10$

and Poisson’s ratio of 0.3 is shown in Figure 10c. It is clear from Figure 10c that as the relative surface energy length increases, the beam deflection decreases w.r.t. that predicted by Timoshenko’s beam theory, which is an indication of a “beam rigidity effect”. This effect is attributed to the surface energy term that as in the case of the half-space problem treated in Paragraph 1.5 gives rise to a pre-tensioning of the beam.

2.7 Size effect of beam strength

Assuming that the *Poncelet - Saint Venant (PSV) failure hypothesis* is valid for granular brittle materials, then the fracture of the beam will occur when the horizontal extension strain at the mid-span of the bottom face of the beam denoted here as ϵ_{xx}^{\max} , reaches the limit strain ϵ_f

$$\epsilon_{xx}^{\max} \geq \epsilon_f \quad \text{at} \quad \zeta = 0, \quad z = \frac{H}{2} \tag{99}$$

where H is the height of the beam. Considering that $\epsilon_{xx} = \kappa z$, then substituting the value of the bending curvature at mid-span found by Equation 97 and multiplying with the modulus of elasticity E, the failure stress at the lower fiber of the beam is found as follows

$$\sigma_{bu} = E\epsilon_f = E \frac{H}{2} \kappa(0) = \sigma_{bu}^{B-E} \frac{\eta^2}{\eta^2 - 1} \left\{ 1 + \frac{2\ell_s}{\eta^2} \frac{1}{L} \right\} \tag{100}$$

wherein σ_{bu}^{B-E} denotes the well-known quantity of Modulus of Rupture of the beam that is given by the formula of the classical Bernoulli-Euler beam bending theory by assuming again the validity of the *PSV failure hypothesis*

$$\sigma_{bu}^{B-E} = E\epsilon_{xx}^{\max} = \frac{P_f LH}{8I} \tag{101}$$

In the formula above, P_f denotes the value of the concentrated load at failure. For constant beam aperture ratio L/H , the following three observations could be made from Equation 100, *i.e.*: (i) Timoshenko’s theory does not predict a size effect and simply modifies the modulus of rupture, (ii) the extended beam bending theory accounting for surface effects, predicts a (-1)- power of the beam length dependence of the flexural strength of the beam, and (iii) this size effect law resembles Karmarsch’s empirical law also used later by Griffith (*i.e.* Equation 1).

The above size effect law was investigated with a series of 3PB experiments with prismatic marble beams with square cross-section (*i.e.* B=H) of Dionysos marble of the same aperture $L/H \cong 4$ but with various spans L ranging from 7.4 cm up to 1 m. This range is considered to be significant for standard rock mechanics tests. Strains at various locations on the beams including their lower surface at the mid-span, were recorded by virtue of electrical strain-gages. More data referring to 3PB experiments on Dionysos marble are provided in Exadaktylos *et al.* (2001b). As is illustrated in Figure 11, the rupture strength calculated according to Equation 101, apart from some dispersion of results for a given aperture ratio that is expected for crystalline brittle

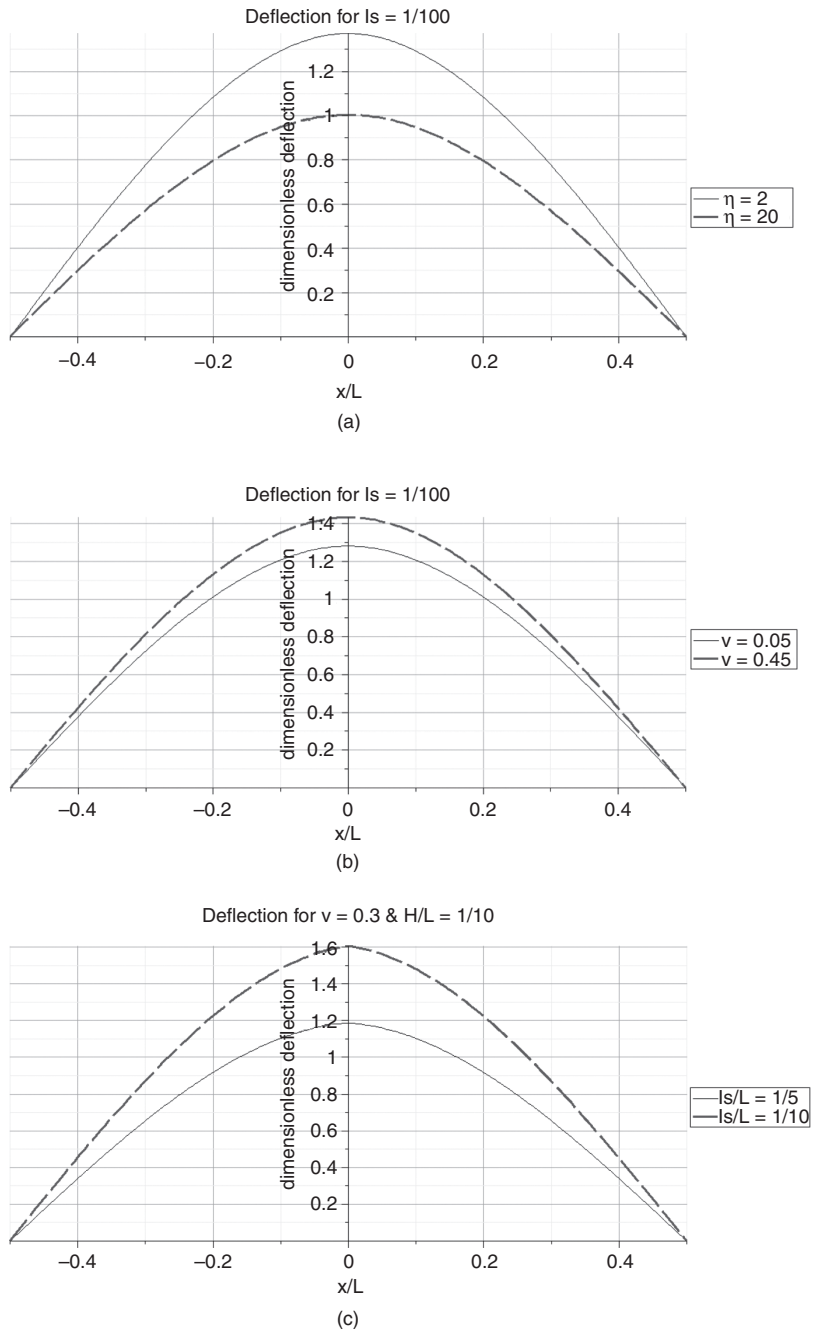


Figure 10 Distribution of beam deflection in 3PB; (a) effect of (H/L) on beam deflection curve for constant Poisson's ratio and surface energy term (i.e. $H/L=1/10$ for the continuous line and $H/L=1/1000$ for the dashed line), (b) effect of Poisson's ratio on beam deflection curve for constant $(H/L=1/10)$ and surface energy term, and (c) effect of surface energy term on beam deflection curve for constant (H/L) and Poisson's ratio.

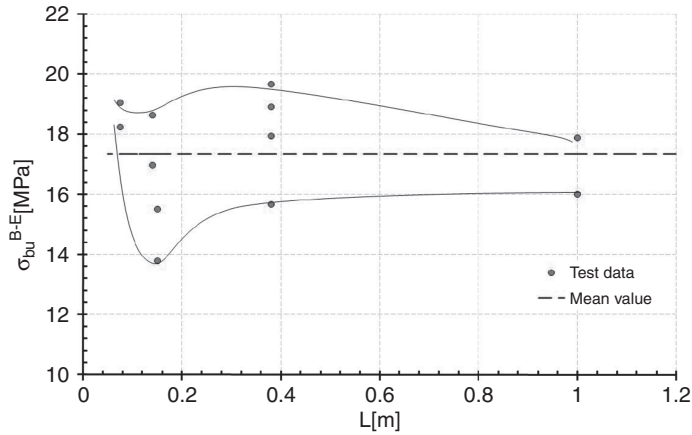


Figure 11 Variation of the modulus of rupture of Dionysos marble for various beam lengths for constant beam aspect ratio $L/H \cong 4$.

materials, was found to be independent of the length of the beam with an average value of $\sigma_{bu}^{B-E} = 17.4 \text{ MPa}$.

Then using Equation 97 and with an elastic modulus of Dionysos marble $E = 85 \text{ GPa}$ (Exadaktylos *et al.*, 2001b), the best-fitted curve on the experimental data assuming the validity of the inverse length of the beam size effect law, was found to have the following form

$$\sigma_{bu} \cong 17.4 + \frac{0.84}{L/m}, \quad \sum_1^{11} (\sigma_a - \sigma_m)^2 = 0.21041 \quad (102)$$

in which the length of the beam is expressed in *m* and σ_{bu} in MPa, and the sum in the right indicates the sum of squared differences between the “actual” data (subscript “a”) and the “model” predictions (subscript “m”).

From Figure 12 it may be seen that the above size effect law fits well the experimental results apart from some overestimation of the relative strength in particular of one of the two tests at $L=1 \text{ m}$ that gives $\sigma_{bu}/\sigma_{bu}^{B-E} \cong 0.7$. This may be attributed to the lower value of $\sigma_{bu}^{B-E} = 16 \text{ MPa}$ found in this test compared to the mean value of $\sigma_{bu} = 17.4 \text{ MPa}$ assumed for the whole size range. However, even this correction gives $\sigma_{bu}/\sigma_{bu}^{B-E} \cong 0.8$, which is much lower than the predicted value of $\sigma_{bu}/\sigma_{bu}^{B-E} \cong 1.0$.

3 FORMATION OF AXIAL SPLITTING CRACKS IN A DEEP ROCK LAYER

3.1 Introduction

Axial splitting phenomena in rocks, *i.e.* tensile fractures, also called joints, which run parallel to the major compression axis, are important in mining and petroleum

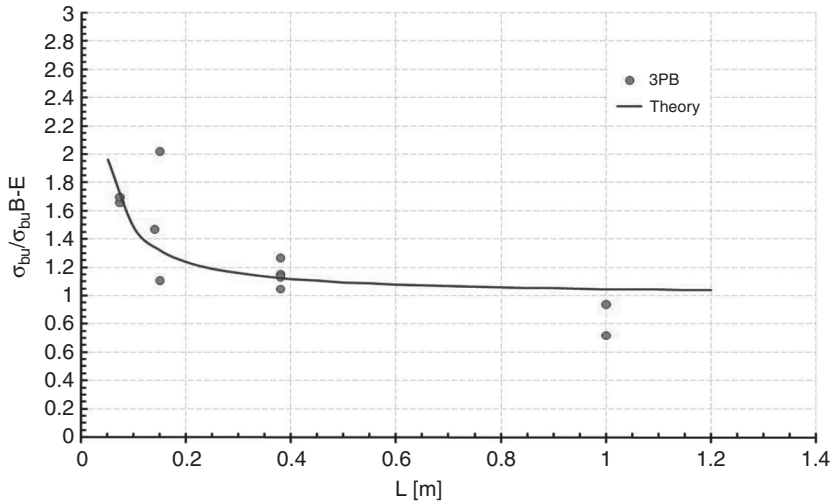


Figure 12 Size effect exhibited by the modulus of rupture of Dionysos marble for constant beam aspect ratio $L/H = 4$.

engineering practices. For example one may mention that deep underground mining results occasionally to explosive “rock bursts” at stope faces in the form of longwall or room and pillar etc. In geological setting, on the other hand, limestone deposits embedded between thin shale layers are characterized by periodic axial splitting, the spatial frequency or spacing of which is very important for permeability estimates. From joint mapping in the field (Bock, 1971, 1980) there are evidences that joints in a geological layer display some kind of periodicity. These layers are transected usually by two main (*haupt*) joint sets that are mutually orthogonal to each other and with spacings exhibiting periodicity. Depending on the case the ratio of the spacing of joints, S , to the thickness of the layer, T , is constant, which means that these two geometrical quantities obey a certain relationship. This ratio S/T varies in most of the cases around the value of two (Bock, 1971, 1980).

In this chapter we consider this problem using two approaches. One refers to the LEFM, and the other refers to the application of bifurcation theory to internal buckling of geological layers under initial stress (Biot, 1965; Vardoulakis & Sulem, 1995). The latter approach is based on the assumption that the critical buckling stress of a continuous medium is that which causes a radical change of the deformational field without a change of the boundary conditions. It is assumed that brittle fracture is affected by strain gradients. The corresponding bifurcation problem is formulated and solved numerically for a rock layer with anisotropic macrostructure and microstructure.

3.2 LEFM model of axial splitting joints in an isolated rock layer

It is assumed that a deep rock layer is uniaxially compressed under the action of in situ vertical stress σ_V as is illustrated in Figure 13. If the layer behaves in a linear elastic fashion and is situated far from free surfaces (like mountain slopes, workings, caverns,

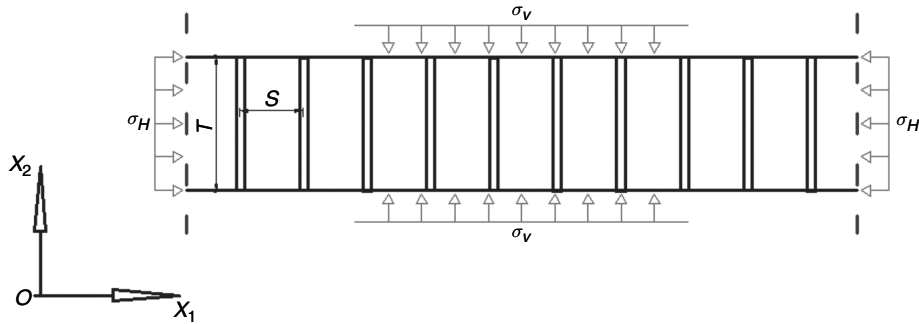


Figure 13 Sketch of a system of parallel periodic axial joints in a horizontal rock layer and Cartesian system of coordinates.

holes etc) deformations in the horizontal directions cannot be realized; therefore the deformation is a constrained uniaxial compression with zero lateral strain *i.e.*

$$\varepsilon_H \approx 0; \quad \sigma_H = K\sigma_V, \quad K = \frac{\nu}{1-\nu} \tag{103}$$

where K denotes the lateral stress ratio.

Based on micromechanical experimental evidences it may be said that in polycrystalline or granular materials like rocks the nonhydrostatic compressive loads generate locally tensile stresses. These local tensile stresses arise from material property mismatches and grain boundary irregularities (Tapponnier & Brace, 1976). In turn, these tensile stresses cause the initiation and propagation of mode-I cracks that are aligned with the major compressive principal stress *i.e.* along Ox_2 axis as is shown in Figure 13 (compressive stresses are considered positive quantities unless stated otherwise). In the configuration of the rock bed subjected to geostatic stresses the mean stress may be found as follows

$$p = \frac{1 + \nu \sigma_V}{1 - \nu} \tag{104}$$

Then it may be shown that the principal deviatoric stresses along the horizontal Ox_1 and the vertical Ox_2 axes are given by the following formulae, respectively

$$s_1 = -\frac{1 - 2\nu}{3} \frac{1 - \nu}{1 - \nu} \sigma_V, \quad s_2 = \frac{2}{3} \frac{1 - 2\nu}{1 - \nu} \sigma_V \tag{105}$$

It may be observed that the horizontal deviatoric stress is tensile, while the vertical deviatoric stress is compressive, which could explain the alignment of the axial splitting cracks along Ox_2 -axis based on the above consideration of local stress concentrations at grain scale.

As is shown in Figure 14a, for the periodic parallel crack problem the mode-I SIF K_I is assumed to be the superposition of the tensile deviatoric stress s_1 properly amplified and of the all-around uniform compression p in the following fashion (from now on we consider tensile stresses and extensional strains as positive quantities)

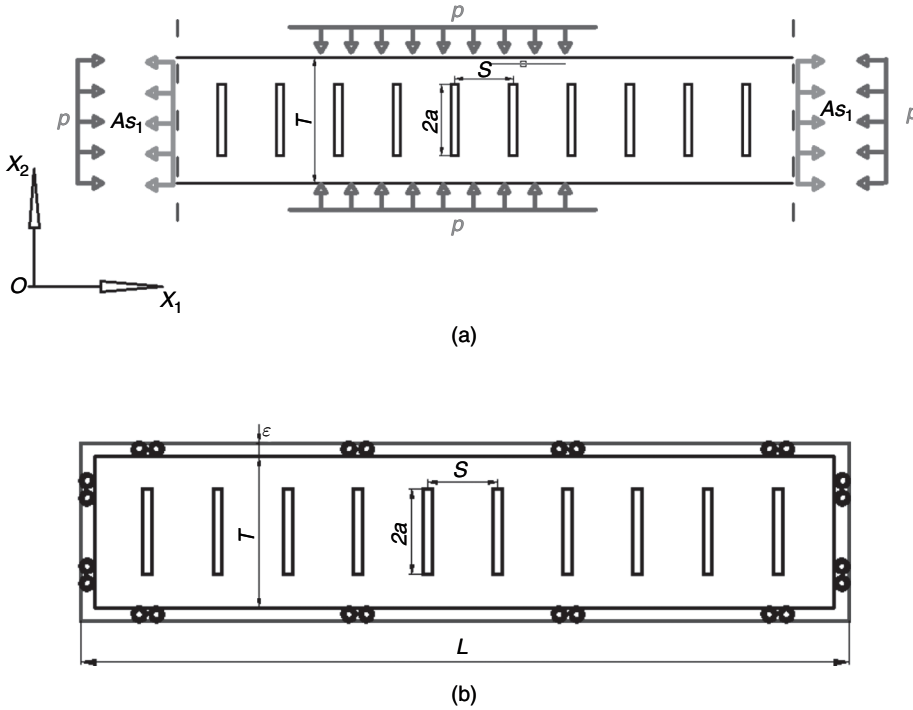


Figure 14 Plane strain model of the infinite layer weakened by parallel periodic axial splitting cracks; (a) Array of periodic and parallel cracks in an elastic layer, and (b) array of parallel joints in a layer of length L with fixed boundaries.

$$K_I = Y\left(\frac{S}{T}, \frac{2a}{T}\right) [A \cdot s_1 + p] \sqrt{\pi a} \quad (106)$$

where Y is a configuration correction factor that is a function of the spacing-to-thickness and crack length-to-thickness ratios, and A is an amplification factor between the local tensile stress and the applied deviatoric stress s_1 (Costin, 1983) that is assumed to be a constant in this model. The SIF due to the deviatoric stress s_2 that acts in a direction parallel with the cracks is obviously null. Chen (2004) has solved the stress boundary value problem of an infinite strip weakened by an array of periodic parallel cracks and has presented numerical values of the mode-I SIF acting on the crack tips of the axial cracks for various values of the ratios S/T and $2a/T$. The regression analysis of his results performed herein has been accomplished by using the following interpolation function for the configuration correction factor Y

$$Y\left(\frac{S}{T}, \frac{2a}{T}\right) = x_1 \left(\frac{2a}{T}\right)^2 + x_2 \left(\frac{2a}{T}\right) + x_3 \left(\frac{2a}{T}\right) \left(\frac{S}{T}\right) + x_4 \left(\frac{S}{T}\right) + x_5 \left(\frac{S}{T}\right)^2 + x_6 \quad (107)$$

732 G. Exadaktylos

The regression analysis showed that the following values of the constant coefficients result in a mean error of 3% in the range of values of the two ratios also used to find the numerical values by Chen, *i.e.* $S/T \in [0.4, 2]$ and $2\alpha/T \in [0.1, 0.8]$,

$$\begin{aligned} x_1 = 2.4369, \quad x_2 = -1.4272, \quad x_3 = 0.1497, \\ x_4 = 0.5390, \quad x_5 = -0.2058, \quad x_6 = 0.8533 \end{aligned} \tag{108}$$

The above solution is not representative for the bed that lies at great depth below the free surface. Instead the most appropriate boundary conditions for the bed are fixed displacements as is shown in Figure 14b. The compliance of the cracked layer with clamped boundaries is depicted partly from the cracks and partly from the intact rock,

$$\varepsilon = C\sigma + \frac{1}{E}\sigma, \quad \sigma = As_1 + p \tag{109}$$

where C is the compliance of the cracked bed. The additional strain energy due to N cracks is given by the formula below

$$\Delta U_a = \frac{TL}{2}\sigma\varepsilon = \frac{TL}{2}C\sigma^2 \tag{110}$$

Irwin (1957) has proved the following relationship that is valid under fixed grips, plane strain conditions and mode-I cracks

$$\frac{\partial \Delta U_a}{\partial \alpha} = \frac{(1 - \nu^2)}{E} K_I^2 \tag{111}$$

By virtue of Equations 110 and 111 and integrating we get the expression for the compliance of the elastic layer due to $N = L/s$ cracks

$$C = \frac{2\pi(1 - \nu^2)N}{TLE} \left(-A \frac{1}{3} \frac{1 - 2\nu}{1 - \nu} + \frac{1}{3} \frac{1 + \nu}{1 - \nu} \right)^2 \int_0^\alpha \alpha Y^2 da \tag{112}$$

Subsequently from Equation 109 the stress-strain relationship may be derived as follows

$$\sigma = \frac{E\varepsilon}{1 + \frac{2\pi(1 - \nu^2)N}{TL} \left(-A \frac{1}{3} \frac{1 - 2\nu}{1 - \nu} + \frac{1}{3} \frac{1 + \nu}{1 - \nu} \right)^2 \int_0^\alpha \alpha Y^2 da} \tag{113}$$

The definite integral appearing in the above expression may be easily computed in closed form from the polynomial Equation 109 of the configuration correction factor. Finally, the SIF may be derived from Equations 106 and 113 in the following manner

$$\begin{aligned} K_I = Y\sqrt{\pi a} \times \\ \times \frac{E\varepsilon}{1 + \frac{2\pi(1 - \nu^2)N}{TL} \left(-A \frac{1}{3} \frac{1 - 2\nu}{1 - \nu} + \frac{1}{3} \frac{1 + \nu}{1 - \nu} \right)^2 \int_0^\alpha \alpha Y^2 da} \end{aligned} \tag{114}$$

A dimensionless SIF may be defined by setting $\sigma_0 = E\varepsilon$ in the following fashion $K_I/\sigma_0\sqrt{\pi T}$. Using Equation 110 the elastic strain energy of the cracked geological layer with N joints of length 2α under certain macro-strain ε becomes

$$U_a = \frac{1}{2} \frac{ELT\varepsilon^2}{1 + \frac{2\pi(1-\nu^2)N}{TL} \left(-A \frac{1}{3} \frac{1-2\nu}{1-\nu} + \frac{1}{3} \frac{1+\nu}{1-\nu} \right)^2 \int_0^\alpha \alpha Y^2 da} \quad (115)$$

The determination of the equilibrium crack length in the elastic bed with fixed displacement is then based on the following three criteria proposed by Kemeny & Cook (1985),

$$\begin{aligned} K_I &= K_{IC}, \\ \frac{\partial K_I}{\partial \alpha} &< 0, \\ \min U_a \end{aligned} \quad (116)$$

The third ad hoc criterion postulated by Kemeny & Cook (1985) and is shown in Equation 116 means that for a given strain ε applied to the rock layer, rock parameters ν , A , K_{IC} and bed thickness T , the optimum configuration will be such that minimizes the stored elastic strain energy U_a . Figure 15 illustrates the variation of the dimensionless SIF with the crack semi-length to bed thickness ratio for various values of crack spacing to bed thickness ratios and for a constant Poisson's ratio $\nu = 1/3$ and amplification factor $A = 20$. As was expected the SIF under fixed-grips conditions is initially increasing with crack length, reaches a peak and then decreases monotonically since the stress is released due to increasing crack length. As it may be seen from Figure 15 below as the number N of cracks increases – for fixed bed length L this means a decreasing S/T ratio – the equilibrium crack length decreases. According to the second crack propagation criterion the equilibrium crack length is found by the intersection of the respective curve with the fracture toughness line that is parallel to the horizontal axis. Employing the third criterion of the minimization of the stored strain energy then as may be seen in Table 1. it turns out that the optimum configuration is established for $S/T \cong 2.2$ as is also observed in reality and crack length comparable to bed thickness. It is remarked here that this model does not predict a size effect, that is to say dependence of the critical strain or stress on the bed thickness, for fixed S/T ratio.

3.3 Internal buckling of a single layer of rock under initial stress

The same problem is considered here as a non-homogeneous, plane-strain deformation of a horizontal layer of thickness T and very large horizontal extent, due to constant vertical compression σ_v as shown in Figure 13. The theory used in this alternative analysis is based on incremental plane strain deformations superimposed on the large strain of a uniform compression. For the considered non-homogeneous deformation mode, we seek such a displacement field that displays certain periodicity along Ox_1 and Ox_2 axes. An appropriate periodical deformation field would be such that: a) along the vertical axis Ox_2 the joints open, b) the deformations attenuate until the middle of the

Table 1 Dependence of the dimensionless elastic strain energy for the various values of crack spacing to bed thickness and crack length to bed thickness ratios.

S/T	$2a/T$	$U_a/E\epsilon^2T^2$
0.4	0.15	0.918
1	0.36	1.326
2	0.82	0.972
2.2	0.92	0.876

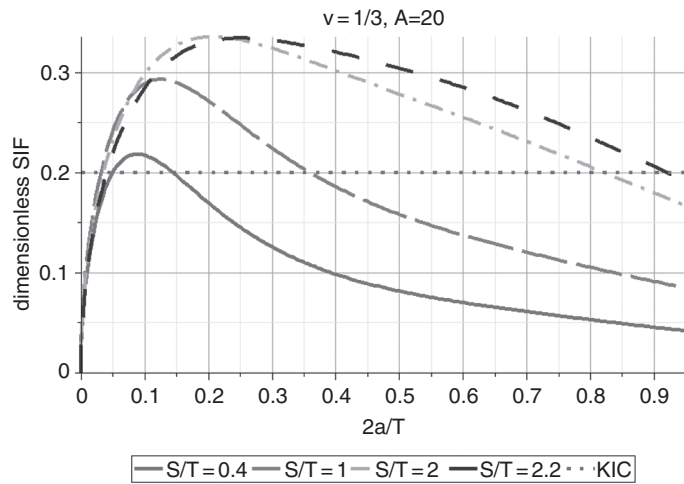


Figure 15 Dependence of the dimensionless SIF on the crack length to bed thickness ratio for various number of cracks or crack spacing to bed thickness ratio for $\nu = 0.3$, $A=20$ and $K_{IC}/\sigma_0\sqrt{\pi T} = 0.2$.

distance to the neighboring cracks, c) it corresponds to the locations of the joints, and d) it is given in terms of two unknown amplitude functions of the dimensionless coordinate x_2 ,

The sine and cosine functions are the most appropriate to describe the deformational field prescribed above (Biot, 1965), that is essentially the deformational pattern of a “standing wave”. Hence the following expressions for the displacement components are employed

$$\begin{aligned} V_1 = \Delta u_1 &= A \sin(a_n x_1) \cos(b_m x_2) \\ V_2 = \Delta u_1 &= B \cos(a_n x_1) \sin(b_m x_2) \end{aligned} \tag{117}$$

where we have set

$$a_n = \pi \frac{n}{S}, \quad b_m = \pi \frac{m}{T} \tag{118}$$

with n, m being even natural numbers, and the dimensionless coefficients A, B denoting the displacement amplitudes. Figures 16a illustrate the deformation modes of the geological layer weakened by periodic parallel axial splitting joints for the cases $n=1$,

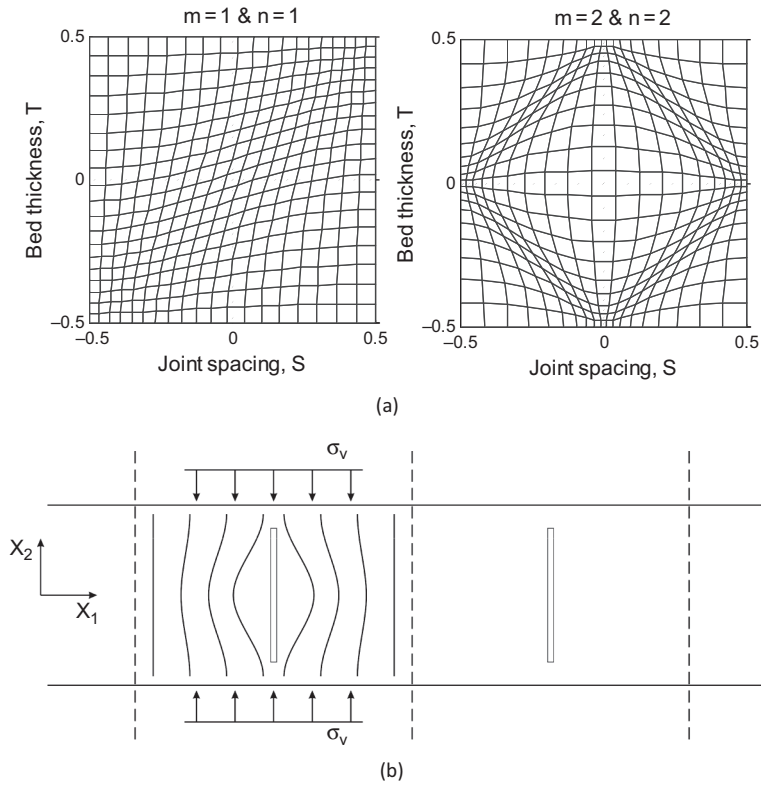


Figure 16 (a) Deformational modes of the geological layer for $n=1, m=1$ (left) and $n=2, m=2$ (right), and (b) lines of equal horizontal strain around the joint.

$m=1$ and $n=2, m=2$. Figure 16b shows the deformation field around each vertical axial joint.

It is assumed that the elasticity of the geological layer displays a cubic symmetry that is described with three elasticity constants instead of the usual two constants of isotropic elasticity (Landau & Lifshitz, 1975). Cubic materials possess a shear modulus denoted here with the symbol G that is not related to the Young's modulus and Poisson's ratio with the usual relation of isotropic elasticity. The ratio G/G^* is used here as a measure of anisotropy of the geological material, *i.e.*

$$\frac{2(1+\nu)}{E}G = \frac{G}{G^*} = \zeta_2 \quad (119)$$

This anisotropy of the macrostructure is essential for the modeling of the axial splitting fracture of the layer, as is the deviatoric stresses with large enough amplification factor A assumed in the frame of the LEM approach presented previously. Assuming infinitesimal strain elasticity, the Jaumann stress increments $\Delta^\circ \sigma_{ij}$ of the total stress are related directly to the strain increments $\Delta \varepsilon_{ij}$ through the constitutive relations of linear elastic materials, perturbed properly in order to account for higher order strain gradients and anisotropy in the microstructure (Exadaktylos & Vardoulakis, 1998)

$$\begin{aligned}
 \overset{\circ}{\Delta} \sigma_{11} &= \frac{2G^*}{1-2\nu} \{ (1-\nu)\Delta\varepsilon_{11} + \nu\Delta\varepsilon_{22} \} - 2G\ell^2 \nabla^2 \Delta\varepsilon_{11} \\
 \overset{\circ}{\Delta} \sigma_{22} &= \frac{2G^*}{1-2\nu} \{ \nu\Delta\varepsilon_{11} + (1-\nu)\Delta\varepsilon_{22} \} - 2G\ell^2 \nabla^2 \Delta\varepsilon_{22} \\
 \overset{\circ}{\Delta} \sigma_{12} &= \overset{\circ}{\Delta} \sigma_{21} = 2G \left(\Delta\varepsilon_{12} - \ell^2 \nabla^2 \Delta\varepsilon_{12} \right)
 \end{aligned} \tag{120}$$

In this first attempt we simplify considerably the problem at hand by assuming that the strain gradients affect only the horizontal stress increment in the following manner,

$$\begin{aligned}
 \overset{\circ}{\Delta} \sigma_{11} &= \frac{2G^*}{1-2\nu} \{ (1-\nu)\Delta\varepsilon_{11} + \nu\Delta\varepsilon_{22} \} - G\ell^2 \Delta\varepsilon_{11,11} \\
 \overset{\circ}{\Delta} \sigma_{22} &= \frac{2G^*}{1-2\nu} \{ \nu\Delta\varepsilon_{11} + (1-\nu)\Delta\varepsilon_{22} \} \\
 \overset{\circ}{\Delta} \sigma_{12} &= \overset{\circ}{\Delta} \sigma_{21} = 2G\Delta\varepsilon_{12}
 \end{aligned} \tag{121}$$

where ℓ is an internal length scale that is used for the consideration of the strain gradient only in the horizontal component of stress, and $\Delta\varepsilon_{ij}$ designates the incremental infinitesimal strain tensor

$$\Delta\varepsilon_{ij} = \frac{1}{2} (\Delta u_{i,j} + \Delta u_{j,i}) \tag{122}$$

Considering that the layer of infinite lateral extent has fixed upper and lower boundaries (internal buckling problem) while the horizontal displacements along the cracks cancel out, plus the symmetry conditions, then the boundary conditions of the internal buckling problem are imposed in the following fashion,

$$\begin{aligned}
 V_1 = 0, \quad \Delta\varepsilon_{12} = 0 \quad \forall x_2 \text{ and } x_1 = \pm l/2 \\
 V_2 = 0, \quad \Delta\varepsilon_{12} = 0 \quad \forall x_1 \text{ and } x_2 = \pm h/2
 \end{aligned} \tag{123}$$

The model given by Equation 117 satisfies the boundary conditions for $n=2$ and $m=2$,

$$\begin{aligned}
 V_1(\pm l/2, x_2) &= A \sin(\pm\pi) \cos(b_m x_2) = 0 \\
 \Delta\varepsilon_{12}(\pm l/2, x_2) &= -\frac{1}{2} (Ba_n + Ab_m) \sin(\pm\pi) \sin(b_m x_2) = 0
 \end{aligned} \tag{124}$$

and

$$\begin{aligned}
 u_2(x_1, \pm h/2) &= B \cos(a_n x_1) \sin(\pm\pi) = 0 \\
 \varepsilon_{12}(x_1, \pm h/2) &= -\frac{1}{2} (Ba_n + Ab_m) \sin(a_n x_1) \sin(\pm\pi) = 0
 \end{aligned} \tag{125}$$

For continuing linear equilibrium in plane strain conditions (*i.e.* $\partial_3 = 0$) and in the coordinate system of principal axes of initial stress σ_{ij} in the plane of the deformation, the stress equilibrium equations take the following form (Biot, 1963)

$$\begin{aligned}
 \overset{\circ}{\Delta} \sigma_{11,1} + \overset{\circ}{\Delta} \sigma_{12,2} + \sigma_\nu \Delta \omega_{21,2} &= 0 \\
 \overset{\circ}{\Delta} \sigma_{21,1} + \overset{\circ}{\Delta} \sigma_{22,2} + \sigma_\nu \Delta \omega_{21,1} &= 0
 \end{aligned} \tag{126}$$

where $\Delta\omega$ being the incremental rotation (spin) tensor

$$\Delta\omega_{ij} = \frac{1}{2}(\Delta u_{i,j} - \Delta u_{j,i}) \tag{127}$$

Substituting Equations 121 & 117 in the equilibrium Equations 126 the following equations are obtained

$$\begin{aligned} C_{11}\Delta\varepsilon_{11,1} + C_{12}\Delta\varepsilon_{22,1} - G\ell^2\Delta\varepsilon_{11,111} + 2G\Delta\varepsilon_{12,2} + \sigma_v\Delta\omega_{,2} &= 0 \\ 2G\Delta\varepsilon_{12,1} + C_{21}\Delta\varepsilon_{11,2} + C_{22}\Delta\varepsilon_{22,2} + \sigma_v\Delta\omega_{,1} &= 0 \end{aligned} \tag{128}$$

where we have set

$$C_{11} = C_{22} = \frac{2G^*(1-\nu)}{1-2\nu}, \quad C_{12} = C_{21} = \frac{2G^*\nu}{1-2\nu} \tag{129}$$

Finally, by employing the strain-displacement and the rotation-displacement Equations 122 and 127, respectively, we obtain the following system of algebraic equations

$$\begin{cases} -\left(A\left(G\ell^2 a_n^4 + C_{11}a_n^2 - \left(\frac{\sigma_v}{2} - G\right)b_m^2\right) + B\left(C_{12} + G + \frac{\sigma_v}{2}\right)a_n b_m\right) = 0 \\ -\left(A\left(C_{21} + G - \frac{\sigma_v}{2}\right)a_n b_m + B\left(C_{22}b_m^2 + \left(G + \frac{\sigma_v}{2}\right)a_n^2\right)\right) = 0 \end{cases} \tag{130}$$

The above system of Equations 130 is further simplified by dividing both equations with the term a_n^2 and with the shear modulus G^* , that is

$$\begin{cases} \left(A\left(\ell_a^2 + c_{11} - (\xi_1 - \xi_2)r^2\right) + B\left(c_{12} + (\xi_1 + \xi_2)r\right)\right)r = 0 \\ \left(A\left(c_{12} - (\xi_1 - \xi_2)r\right)r + B\left(c_{11}r^2 + (\xi_1 + \xi_2)\right)\right) = 0 \end{cases} \tag{131}$$

where we have set

$$\begin{aligned} c_{11} &= C_{11}/G^* = C_{22}/G^*, \quad c_{12} = C_{12}/G^* = C_{21}/G^*, \\ \xi_1 &= \frac{\sigma_v}{2G^*}, \quad \xi_2 = \frac{G}{G^*} \\ \ell_a^2 &= \ell^2 \xi_2 a_n^2, \quad r = \frac{b_m}{a_n} = \frac{Sm}{nT} = \frac{S}{T} \end{aligned} \tag{132}$$

For non-trivial solution in terms of A and B, the determinant of the system of Equations 131 must vanish. This leads to the following biquadratic equation for the aspect ratio of axial joints r , *i.e.*

$$\begin{aligned} r^4 + 2mr^2 + k^2 &= 0, \\ 2m &= \frac{p_2}{p_4} = \frac{c_{11}\ell_a^2 + c_{11}^2 - c_{12}^2 - 2c_{12}\xi_2}{c_{11}(\xi_2 - \xi_1)}, \\ k^2 &= \frac{p_0}{p_4} = \frac{(\ell_a^2 + c_{11})(\xi_2 + \xi_1)}{c_{11}(\xi_2 - \xi_1)} \end{aligned} \tag{133}$$

The roots of Equation 133 are

$$\begin{aligned} r_1^2 &= -m + \sqrt{m^2 - k^2}, \\ r_2^2 &= -m - \sqrt{m^2 - k^2} \end{aligned} \tag{134}$$

A solution is possible if there exists a real root r_i ; that is, if either r_1^2 or r_2^2 or both are positive. This occurs in the following cases: (Case 1) $m > 0$, $k^2 < 0$ in which the root r_1^2 is positive and r_1 is real; (Case 2) $m < 0$, $m^2 > k^2 > 0$ in which both r_1^2 and r_2^2 are positive and so r_1 and r_2 are real.

The critical internal buckling stress is then found as the minimum load ξ_1 for which Equation 133 has real roots. This is illustrated in Figure 17 that presents the dependence of the buckling load on the aspect ratio of the jointed layer for four cases of anisotropy, namely $\xi_2 = G/G^*$ equal to 2.5, 3, 5, and 7, a constant Poisson's ratio $\nu = 0.49$ – since rock masses at great depths behave in an almost incompressible manner – and a dimensionless microstructural length scale $\ell_a = 0.1$. It may be observed that as the macroscopic anisotropy of the layer becomes more pronounced, then both the crack spacing to bed thickness ratio and the buckling load decrease. In general, both the aspect ratio of axial splitting cracks and of the buckling load decrease with the increase of the macrostructural anisotropy of the bed or equivalently with the amplification factor A of the tensile stresses acting on the crack tips.

Plots of several spectra of the buckling stress with aspect ratio for various values of the dimensionless microstructural length scale ℓ_a are illustrated in Figure 18a. From these

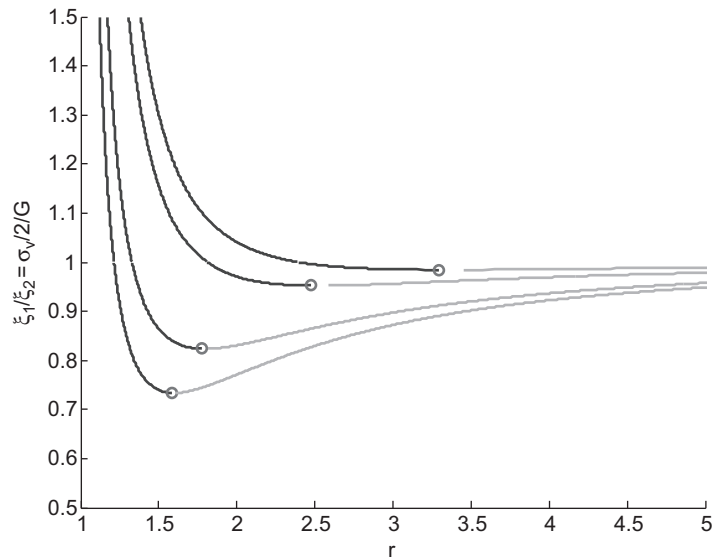


Figure 17 Dependence of the dimensionless buckling load on the aspect ratio of the crack spacing to bed thickness for $\nu=0.49$ and for four shear moduli $\xi_2 = G/G^*$ equal to 2.5, 3, 5, and 7, respectively and constant internal length scale. The global minima represented by the circles are moving toward the left of the diagram as ξ_2 increases.

plots it may be drawn the interesting result referring to the dependence of the buckling load on the crack spacing to bed thickness ratio for any specified degree of anisotropy of the macrostructure, shown in Figure 18b, that is a manifestation of a size effect.

Indeed, a size effect law of the following form was best-fitted on the numerical data presented in Figure 18b,

$$\xi_1 = C_1 \left(\frac{r}{\ell_a} \right)^{-\beta} + C_0 \tag{135}$$

where C_1 , C_0 , β are constant factors. In fact C_0 is the buckling load for $\ell_a \rightarrow 0$. Then by combining Equation 135 and the third of Equation 132, it may be seen that the size effect of the buckling load on the spacing of cracks for constant aspect ratio, anisotropy ratio and internal length scale takes the form

$$\xi_1 = \left[C_1 \left(\frac{S}{T} \right)^{-\beta} \left(4\pi \sqrt{\xi_2} \ell \right)^\beta \right] S^{-\beta} + C_0 \tag{136}$$

The regression analysis of the numerical data by using the power-law given by Equation 135 gave the following values of the constant coefficients

$$C_1 = 1.4476, \beta = 2.1748, C_0 = 6.048 \tag{137}$$

It may be seen that the exponent is relative large and explains the fact that in real situations it is very rare that the ratio of axial splitting joints spacing relatively to the bed thickness is less than unity.

4 SUMMARY

After a brief overview of some applications of the Casal-Mindlin microelasticity or grade-2 or second gradient of strain theory with surface energy, for the study of fundamental static and dynamic problems, two problems are thoroughly presented here, namely the bending of beams and the axial splitting of deep geological layers. In all cases that were reviewed and examined, it is demonstrated that the consideration of internal length scales are responsible for the manifestation of size effects in static problems and non-classical dispersion phenomena in dynamic problems.

More specifically, it was illustrated that the surface energy term of the technical beam theory is responsible for a size effect exhibited by the flexural strength of beams in three-point bending, namely the dependence of the flexural strength on the inverse length of the beam for the same aspect ratio. Based on the assumption that the failure extensional strain in bending is equal to the failure extensional strain in direct or indirect tension, and the assumption of a linear elastic behavior of the brittle material up to failure, then also a L^{-1} size effect of the tensile strength of quasi-brittle solids in direct as well as in indirect tensile tests, has been derived. The size effect predicted by the proposed theory is validated against experimental results of beam bending of Dionysos marble.

It has been also found the interesting result referring to the dependence of the buckling load of a rock bed transected by periodic system of axial splitting cracks on

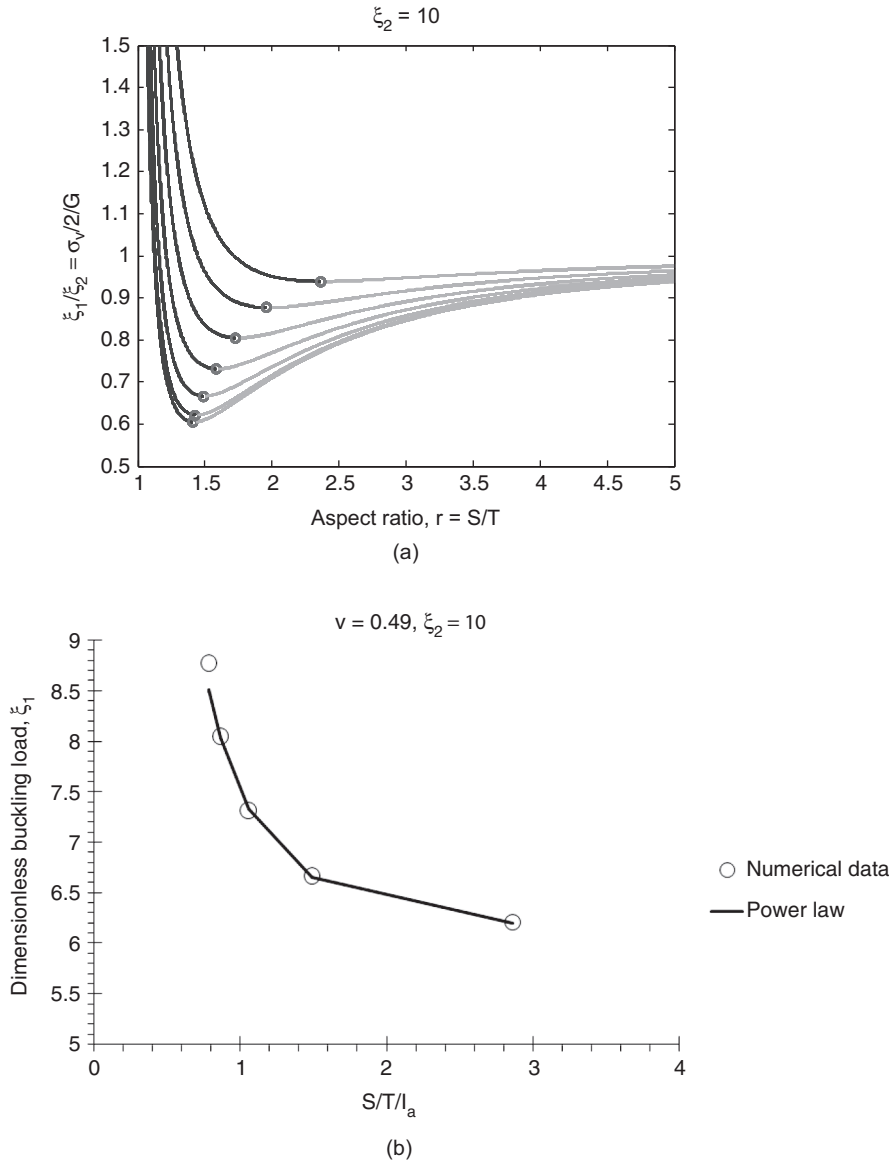


Figure 18 (a) Dependence of the dimensionless buckling load represented by the circles on the aspect ratio of joints for various microstructural length scales (as the microstructural scale parameter increases the critical buckling load decreases) for $\xi_2 = 10$ and Poisson's ratio $\nu = 0.49$, and (b) size effect exhibited by the buckling load for $\nu = 0.49$ and $\xi_2 = 10$.

the bed thickness, for fixed crack spacing to bed thickness ratio and a specified degree of anisotropy of the macrostructure.

Hence, there is ample space for further applications of this theory both for the development of computational codes and new experimental techniques that could

take into account the effect of rock microstructure on rock behavior. For example in a series of papers Exadaktylos & Xiroudakis (2009, 2010a,b) have developed a special grade 2 constant displacement discontinuity method – *i.e.* with one collocation point per element – for the accurate solution of plane crack problems. Furthermore, it is important to further develop this theory in the context of nonlinear elasticity and plasticity theories and the development of new failure theories of rocks. Other technologically important problems that may be considered in the frame of the present theory, are the elastic wave propagation in earthquakes and seismic wave characterization of rock masses, and modeling of the mechanical behavior of rock joints and size effects among many others.

REFERENCES


- Achenbach J.D. (1973). *Wave Propagation in Elastic Solids*. Amsterdam, North-Holland.
- Aifantis E.C. (1992). On the role of gradients in the localization of deformation and fracture. *Int. J. Eng. Sci.*, 30, 1279–1299.
- Aravas N. (2011). Plane-strain problems for a class of gradient elasticity models—A stress function approach. *J. Elast.*, 104, 45–70.
- Biot M.A. (1963). Internal buckling under initial stress in finite elasticity. *Proc. R. Soc. London, Ser. A*, A273, 306–328.
- Biot M.A. (1965). *Mechanics of Incremental Deformations*. John Wiley & Sons, New York (1965).
- Bock H. (1980). Das Fundamentale Kluftsystem. *7dt. Geol. Ges.*, 131, 627–650, Hannover.
- Bock H. (1971). Geländebeobachtungen ueber Klueftung in tectonisch wenig beanspruchten Sedimentgesteinen, Int. Symposium Soc., Mecanique des Roches, Nancy, pp. 1–11.
- Casal P. (1961). La capillarité, interne. *Cahier du Groupe Français d'Etudes de Rhéologie* C.N.R. SVI no. 3, 31–37.
- Chen Y-Z (2004). Stress analysis for an infinite strip weakened by periodic cracks. *Appl. Math. Mech.*, 25(11), 1298–1303.
- Cosserat E. & Cosserat F. (1909). *Théorie des corps déformables*. A. Herman et Fils, Paris.
- Costin L.S. (1983). A microcrack model for the deformation and failure of brittle rock. *J. Geophys. Res.*, 88(B11), 9485–9492.
- Coulson C.A. (1958) *Waves*. Oliver and Boyd, Edinburgh and London, Reprinted 1958.
- Currie D.K., Hayes M.A. & O'Leary P.M. (1977). Viscoelastic rayleigh waves. *Q. Appl. Math.*, 35, 35–53.
- Eringen A.C. & Suhubi E.S. (1975). *Elastodynamics*, Volume II, Academic Press, New York and London.
- Exadaktylos G., Vardoulakis I. & Aifantis E. (1996). Cracks in gradient elastic bodies with surface energy. *Int. J. Fract.*, 79, 107–119.
- Exadaktylos G. & Vardoulakis I. (1998). Surface instability in gradient elasticity. *Int. J. Solids Struct.*, 35, 2251–2281.
- Exadaktylos G. (1998). Gradient elasticity with surface energy: Mode-I crack problem. *Int. J. Solids Struct.*, 35, 421–456.
- Exadaktylos G. & Vardoulakis I. (2001a). Microstructure in linear elasticity and scale effects: A reconsideration of basic rock mechanics and rock fracture mechanics. *Tectonophysics*, 335, 81–109.
- Exadaktylos G.E., Vardoulakis I. & Kourkoulis S.K. (2001b). Influence of nonlinearity and double elasticity on flexure of rock beams-II. Characterization of Dionysos marble. *Int. J. Solids Struct.*, 38, 4119–4145.

- Exadaktylos G. & Xiroudakis G. (2009). A G2 constant displacement discontinuity element for analysis of crack problems. *Comput. Mech.*, 45, 245–261.
- Exadaktylos G. & Xiroudakis G. (2010a). The G2 constant displacement discontinuity method – Part I: Solution of plane crack problems. *Int. J. Solids Struct.*, 47, 2568–2577.
- Exadaktylos G. & Xiroudakis G. (2010b). The G2 constant displacement discontinuity method – Part II: Solution of half-plane crack problems. *Int. J. Solids Struct.*, 47, 2578–2590.
- Georgiadis H.G., Brock L.M. & Rigatos A.P. (1998). Transient concentrated thermal/mechanical loading on the faces of a crack in a coupled-thermoelastic solid. *Int. J. Solids Struct.*, 35, 1075–1097.
- Germain P. (1973a). La méthode des puissances virtuelles en mécanique des milieux continus. Part I. *Journal de Mécanique*, 12, 235–274.
- Germain P. (1973b). The Method of virtual power in continuum mechanics. Part 2: Microstructure. *SIAM, J. Appl. Math.*, 25, 556–575.
- Griffith A.A. (1921) The phenomena of rupture and flow in solids. *Philos. Trans. R. Soc. London, Ser. A*, 221, 163–198.
- Guenther W. (1958) Zur Statik und Kinematik des Cosseratschen Kontinuums. In: *Abhandlungen der Braunschweigischen Wissenschaftlichen Gesellschaft*, Göttingen, Verlag E. Goltze, 101, 95–213.
- Irwin G.R. (1957). Analysis of stresses and strains near the end of a crack traversing a plate. *J. Appl. Mech.*, 24, 361–364.
- Jaeger J.C., Cook N.G.W. & Zimmerman R.W. (2007) *Fundamentals of Rock Mechanics*. 4th Edition. Blackwell Publishing.
- Kemeny J. & Cook N.G.W. (1985). Formation and stability of steeply dipping joint sets. *Proceedings of 26th U.S. Symposium on Rock Mechanics*. South Dakota Schools of Mines and Technology, Rapid city, Dakota, 26–28, June, 1985, pp. 471–478.
- Landau L. M. & Lifshitz E.M. (1975). *Theory of Elasticity*. 2nd Edition, Pergamon Press.
- Mindlin R.D., Tiersten H.F. (1962) Effects of couple-stresses in linear elasticity. *Arch. Ration. Mech. Anal.*, 11, 415–448.
- Mindlin, R.D. (1964). Microstructure in linear elasticity. *Arch. Ration. Mech. Anal.*, 10, 51–77.
- Mindlin, R.D. & Eshel, N.N. (1968). On first strain-gradient theories in linear Elasticity. *Int. J. Solids Struct.*, 4, 109–124.
- Papargyri-Beskou S., Tsepoura K.G., Polyzos D. & Beskos D.E. (2003) Bending and stability analysis of gradient elastic beams. *Int. J. Solids Struct.*, 40, 385–400.
- Rayleigh L. (1887). On waves propagated along the plane surface of an elastic solid. *Proc. London Math. Soc.*, 17, 4–11.
- Stavropoulou M., Exadaktylos G.E., Papamichos E., Larsen I. & Ringstad, C. (2003). Rayleigh wave propagation in intact and damaged geomaterials. *Int. J. Rock Mech. Min. Sci.*, 40, 377–387.
- Tapponnier P. & Brace W.F. Development of stress-induced microcracks in westerly granite. *Int. J. Rock Mech. Min. Sci. & Geomech. Abstr.* 13, 103–112. AQ1
- Timoshenko, S.P. (1921). On the correction for shear of the differential equation for transverse vibrations of prismatic beams. *Philos. Mag.*, sec. 6., 41, 744–746.
- Vardoulakis I. (1981). Surface waves in a half-space of submerged sand, *Earthquake Eng. Struct. Dyn.*, 9, 329–342.
- Vardoulakis, I. & Sulem, J. (1995). *Bifurcation Analysis in Geomechanics*. Blackie Academic and Professional.
- Vardoulakis I., Exadaktylos G. & Aifantis, E., (1996). Gradient elasticity with surface energy: Mode III crack problem. *Int. J. Solids Struct.*, 33(30), 4531–4559.
- Vardoulakis I. & Georgiadis H.G. (1997). SH surface waves in a homogeneous gradient-elastic half-space with surface energy. *J. of Elasticity*, 47, 147–165.

- Vardoulakis I., Exadaktylos G.E. & Kourkoulis S.K. (1998). Bending of marble with intrinsic length scales: A gradient theory with surface energy and size effects. *J. Phys. IV France*, 8, 399–406.
- Vardoulakis I. & Giannakopoulos A.E. (2006). An example of double forces taken from structural analysis. *Int. J. Solids Struct.*, 43, 4047–4062.
- Voigt W. (1887). Theoretische Studien ueber die Elasticitaetsverhaeltnisse der Krystalle. *Abb. Ges. Wiss. Goettingen.*, 34.
- Wu C.H. (1992). Cohesive elasticity and surface phenomena. *Q. Appl. Math.*, L(1), 73–103.

AQ2

CHAPTER 23:

S.No.	Page No.	Queries	Remarks
AQ1	742	Please provide the year of publication.	
AQ2	743	please provide the page range details for this reference.	